ISTANBUL TECHNICAL UNIVERSITY ★ GRADUATE SCHOOL OF SCIENCE ENGINEERING AND TECHNOLOGY

SEMI ANALYTICAL PRESSURE SURGE MODEL FOR EXTENDED HERSCHEL-BULKLEY FLUIDS

M.Sc. THESIS

Mücahit YILDIZ

Department of Petroleum and Natural Gas Engineering

Petroleum and Natural Gas Engineering Program

JUNE 2019

ISTANBUL TECHNICAL UNIVERSITY ★ GRADUATE SCHOOL OF SCIENCE ENGINEERING AND TECHNOLOGY

SEMI ANALYTICAL PRESSURE SURGE MODEL FOR EXTENDED HERSCHEL-BULKLEY FLUIDS

M.Sc. THESIS

Mücahit YILDIZ
(505151508)

Department of Petroleum and Natural Gas Engineering

Petroleum and Natural Gas Engineering Program

Thesis Advisor: Assoc. Prof. Dr. Gürşat ALTUN

JUNE 2019

ISTANBUL TEKNİK ÜNİVERSİTESİ ★ FEN BİLİMLERİ ENSTİTÜSÜ

EXTENDED HERSCHEL-BULKLEY AKIŞKANLAR İÇİN YARI ANALİTİK BASINÇ DALGALANMASI MODELİ

YÜKSEK LİSANS TEZİ

Mücahit YILDIZ
(505151508)

Petrol ve Doğal Gaz Mühendisliği Anabilim Dalı

Petrol ve Doğal Gaz Mühendisliği Programı

Tez Danışmanı: Doç. Dr. Gürşat ALTUN

HAZİRAN 2019

Mücahit YILDIZ, an M.Sc. student of ITU Graduate School of Petroleum and Natural Gas Engineering student ID 505151508, successfully defended the thesis entitled "SEMI ANALYTICAL PRESSURE SURGE MODEL FOR EXTENDED HERSCHEL BULKLEY FLUIDS", which he prepared after fulfilling the requirements specified in the associated legislations, before the jury whose signatures are below.

Thesis Advisor:	**Assoc. Prof. Dr. Gürşat ALTUN** İstanbul Technical University
Jury Members:	**Assoc. Prof. Dr. Murat ÇINAR** İstanbul Technical University
	Asst. Prof. Dr. Ali ETTEHADİ İzmir Katip Çelebi University

To my grandfather

FOREWORD

I would like to thank my advisor Dr. Gürşat Altun for guiding and challenging me over the years. Also, I would like to thank Dr. Semra Ahmetolan for giving a point of view to complex mathematical problems. Last but not least, I would especially like to thank my friends, research assistants Muhammed Said Ergül and Gizem Hazal Yıldırım for their constant enthusiasm and encouragement that made this thesis possible.

June 2019

Mücahit YILDIZ
Petroleum and Natural Gas Engineer

TABLE OF CONTENTS

Page

ABBREVIATIONS

BP **:** Bingham Plastic

FPL **:** Frictional pressure loss

HB **:** Herschel-Bulkley

HBE **:** Extended Herschel-Bulkley

PL **:** Power-Law

SYMBOLS

A	:	Area, m^2 (ft^2)
Cc	:	Correction coefficient for the pipe
Ca	:	Correction coefficient for the annulus
d :	:	Internal pipe diameter, m (in.)
$\mathbf{d_1}$	:	Inside diameter of the inner pipe, m (in.)
$\mathbf{d_2}$	:	Outside diameter of the outer pipe, m (in.)
$\frac{dp_f}{dL}$	:	Frictional pressure gradient, Pa/m (Psi/ft)
f	:	Friction factor, fraction
$\mathbf{f_a}$	:	Flow rate ratio, fraction
h	:	Height, m (ft)
K	:	Consistency index of the fluid, $Pa.s^n$ ($lbf.s^n/100sq.ft$)
L	:	Measured length, m (ft)
m	:	Local gradient
n	:	Fluid behavior index
$\mathbf{r_1}$	:	Inner radius of annulus, m (in.)
$\mathbf{r_2}$	:	Outer radius of annulus, m (in.)
r	:	Inside drill pipe annulus, m (in.)
Re	:	Reynolds Number
S	:	Plasticity, dimensionless
q	:	Flow rate, m^3/s (ft^3/s)
$\bar{v}$	:	Mean flow velocity, m/s (ft/s)
$\bar{v}_a$	:	Mean annular flow velocity, m/s (ft/s)
$\mathbf{v_{ae}}$	:	Effective annular flow velocity, m/s (ft/s)
$\mathbf{v_{ae}}$	:	Effective fluid velocity, m/s (ft/s)
$\mathbf{v_p}$	:	Pipe velocity, m/s (ft/s)
w	:	Width, m (ft)
ρ	:	Fluid density, kg/m^3 (lbm/gal)
φ	:	Conductance, dimensionless
μ	:	Fluid viscosity, Pa.s (cp)
μ_p	:	Fluid plastic viscosity, Pa.s (cp)
μ_∞	:	Constant fluid viscosity, Pa.s (cp)
Δp	:	Pressure drop, Pa (psi)
τ	:	Shear stress, Pa (lbf/100sq.ft)
τ_y	:	Yield Point, Pa (lbf/100sq.ft)
γ	:	Shear rate, s^{-1}
λ_1	:	Boundary coefficient for the inner layer, fraction
λ_2	:	Boundary coefficient for the outer layer, fraction

LIST OF TABLES

Page

LIST OF FIGURES

Page

SEMI ANALYTICAL PRESSURE SURGE MODEL FOR EXTENDED HERSCHEL-BULKLEY FLUIDS

SUMMARY

In oil and gas industry, the estimation of surge and swab pressures is crucial since extensively high surge pressures are produced during tripping operations. During the activities that comprise tripping operation for instance pulling a worn-out bit or performing logging tools etc., pipe is run into wellbore or pulled out from wellbore. Since most "easy" wells have been drilled and only "difficult" wells are left, problems in conjunction with surge and swab pressures may cause some expensive drilling troubles for example fluid influx, lost circulation, and kick. Since these challenging wells have quite limited pressure margins, a precise model is required to design drilling applications. In these critical wells, the appropriate estimation of surge and swab pressure can decrease operation costs by saving time and preventing related problems.

In the literature, presented surge and swab models have been developed for mostly Bingham plastic (BP) and Power-law fluids (PL). Still, these rheological models cannot sufficiently characterize the flow behavior of drilling fluids applied in the field. The Hershel-Bulkley (HB) model accurately characterizes the rheology of most drilling fluids. In spite of its great efficiency in predicting the drilling fluid properties, HB model cannot characterize some behavior of drilling fluids at high shear rates. That behavior of fluids can be explained by Extended Herschel-Bulkley (HBE) model. Even though great numbers of non-Newtonian model were conducted by researchers until now to determine surge/swab pressures, HBE has never been used to predict surge/swab pressures.

Field analyses show that surge and swab pressures are greatly associated with fluid rheology, flow regime, wellbore geometry, and open-ended or closed-ended pipe. This study introduces a new steady-state semi analytical model in laminar flow regime by using narrow slot approximation to determine surge and swab pressures due to axial movement of inner pipe for HBE fluids. The analytical solution consists of dealing with a complex non-linear differential equations. That non-linearity has been treated by assuming exponent (n) is constant at 0.5. Mathematical development leads to three equations with three unknowns; the distance of region boundaries and the frictional pressure gradient. These three equations have been solved by Python code using Trust Region Reflective algorithm, particularly suitable for large sparse problems with bounds.

Finally, developed new semi analytical surge and swab model has been tested with both uniform (open-ended) and non-uniform well geometry. The results are validated by comparing with the other models developed for other types of non-Newtonian fluids, particularly for BP and HB.

EXTENDED HERSCHEL-BULKLEY AKIŞKANLAR İÇİN YARI ANALİTİK BASINÇ DALGALANMASI MODELİ

ÖZET

Petrol ve doğal gaz endüstrisinde, sondaj maliyetlerinin çok fazla olmasından dolayı sondaj hızı çok önemlidir. Ne kadar hızlı sondaj yapılırsa maliyet o kadar düşer. Petrol fiyatlarının düşük olduğu zamanlar ise hızın önemi daha da artar. Bunun yanı sıra, ilk petrol üretim tarihinin 100 yıldan fazla olduğunu göz önüne alırsak, dünyadaki çoğu sondajı kolay olan kuyuların yapıldığını ve geriye çoğunlukla sondajı zor ve maliyeti fazla olan, yüksek teknoloji kullanılarak üretimin yapılabildiği kuyular kaldığını söyleyebiliriz. Zamandan kazanmak şimdiye kadar hiç bu kadar önemli olmamıştı. Petrol ve doğal gaz sondajlarında en çok zaman harcanan operasyonlardan birisi de manevra operasyonlarıdır. Diziye boru eklenmesi, kuyu içerisinde sıkışmış parçaların dışarı çıkarılması, aşınmış matkabın değiştirilmesi ve kuyu bilgilerinin alındığı kuyu ölçüm aletlerinin kuyuya indirilmesi ve çıkarılması, bu manevra operasyonlarından bazılarıdır. Sondaj dizisinin, bu manevra operasyonları gerçekleştirmek için, kuyu içerisine veya kuyudan yukarıya doğru hareketinde basınç dalgalanmaları oluşur. Sondaj dizisinin kuyuda aşağı indirilmesi sonucu diziye bitişik durumdaki akışkanı da beraberinde aşağı sürükler. Orta kısımda ki akışkan ise tam tersi yönde yukarı doğru yükselir ve "surge" olarak adlandırılan kuyu içi hidrostatik basıncın artmasına neden olur. Sondaj dizisinin kuyudan yukarı çekilmesi durumunda ise, diziye bitişik olan akışkanı da yukarıya doğru sürükler. Diziden uzak olan akışkan ise tam tersi yönde aşağıya doğru yönelir ve "swab" olarak adlandırılan kuyu içi hidrostatik basıncının azalmasına neden olur. Bu hidrostatik basınç değişiminden sonra basınç dengesi sağlanamazsa çok ciddi sorunlara neden olabilir. Manevra hızını maksimum seviyeye getirebilmek için bu basınç dalgalanmalarının doğru bir şekilde hesaplanması gerekir. Bahsi geçen sondaj sorunlarını minimuma indirmek için formasyon basıncı ile formasyon çatlatma gradyanı arasında güvenlik sınırı vardır. Ancak derindeniz, yüksek eğimli ve yatay kuyularda bu marjin oldukça dardır. O yüzden, basınç dalgalanmalarının en doğru yöntemle hesaplanması hem maliyeti düşürür hem de basınç değişiminden kaynaklanabilecek sorunlarının da önüne geçer.

Basınç dalgalanmalarının bulunmasında seçilen reolojik model çok önemli bir yere sahiptir. Reolojik modeller akışkanın kayma gerilimi (shear stress) ile kayma hızı (shear rate) ilişkisini kullanarak akışkanlarının davranışını tanımlar. Akışkanlar bu davranışlarına göre ideal ve ideal olmayan akışkanlar olmak üzere ikiye ayrılır. Newtonian akış gösteren sistemlerde kayma gerilimi (shear stress) kayma deformasyonunun değişme hızı ile (shear rate) orantılı olarak artmaktadır. Newtonian olmayan sıvıların akış davranışları geniş bir aralıkta olabilir. Temel karakteristikleri, viskozitenin kayma hızı (shear rate) ile doğrudan orantılı olmamasıdır. Diğer bir deyişle, viskozite kayma hızı ile değişir. Newtonian akış göstermeyen bazı sıvılar, zamana bağlı olarak da değişiklik gösterirler. Modern reolojinin araştırıcılarından olan Bingham'ın adına izafeten Bingham plastik akış olarak adlandırılan akışkanın, plastik akış eğrisi orijinden geçmez. Bu tip sıvılar hemen akmazlar ve kayma gerilimi belli bir

eşik değerine (yield value) ulaşınca akış görülür. En çok kullanılan ideal olmayan akışkanlar Bingham plastic, Power-law ve Herschel-Bulkley akışkanlarıdır. Sondaj akışkanlarının davranışı bu ideal olmayan modellerle tanımlanabilir. Ancak sondaj akışkanları birçok akışkanın karışımı olduğu için tek bir model kullanılarak reolojik davranışını tanımlamak yerine bu modellerin birleşimini kullanarak akışkanın reolojik davranışını tanımlamak daha doğru sonuç verir. Basınç dalgalanmalarını öngörebilmek için yapılan çalışmalar çoğunlukla Bingham plastic ve Power-law akışkanları için olmuştur. Ama bu reolojik modeller sahada kullanılan sondaj akışkanın davranışını tanımlamada yetersizdir. Çoğu Sondaj akışkanının davranışını en doğru şekilde tanımlayan model Herschel-Bulkley modelidir. Herschel-Bulkley modelin sondaj akışkanının özelliklerini öngörmesindeki etkisine rağmen yüksek kayma hızlarındaki akışkan davranışını tanımlamada yetersizdir. Bazı sondaj akışkanlarının yüksek kayma hızlarında akışkan akmazlığı sabitlenir. En yüksek kayma hızının matkap uçlarında olmasından dolayı en çok etki orada gözlemlenebilir. Akışkanların yüksek kayma hızındaki bu davranışı genişletilmiş Herschel-Bulkley (HBE) model ile açıklanabilir. Basınç dalgalanmalarının öngörülmesi ile ilgili günümüze kadar birçok çalışma olmasına rağmen, genişletilmiş Herschel-Bulkley model kullanılarak basınç dalgalanmalarının öngörülmesi ile ilgili bir çalışma henüz yapılmamıştır. HBE akışkanları ile ilgili literatürde yeterli çalışma olmadığı gibi yeterli reolojik veri de bulunmamaktadır. Bu yüzden akmazlık okumaları kullanılarak model parametreleri Matlab kodu ile hesaplanmıştır. HBE akışkanları yüksek kayma hızlarında etkili olduğu için 6 kayma hızı kullanılarak hesaplanan parametrede negatif değer bulunmuştur. Bu nedenden dolayı 4 kayma hızı (100 rpm den 600 rpm) kullanılarak BP, HB ve HBE akışkanları için olan parametreler kullanılmıştır.

Bir sistemin reolojik özelliklerinin başarılı bir şekilde ölçülmesi ve değerlendirilmesi, uygun yöntemin ve doğru bir viskometrenin seçilmesine bağlıdır. Viskometrelerin tasarımında, sıcaklık ve işlem parametreleri esas alınır. Bir viskometrenin de, kalite kontrolü için ürünün akış özelliklerini tayin etmesi ve ölçümü yapılacak, örneğin tüp, şişe ve kavanozdan kolaylıkla ve kısa zamanda doğru ölçümünü sağlaması gerekir. Reolojik ölçümlerde amaç, gerilim ve kayma hızı ve bazı durumlarda viskoelastisite arasındaki fonksiyonel ilişkiyi tayin etmektir. Newtonian akış gösteren sistemlerde hız gradyanı ile gerilim arasında doğrusal bir ilişki bulunmaktadır. Bu nedenle, bu tip sistemlerin akış özelliğini ve viskozitesini tayin etmek için tek noktalı viskometreler kullanılmaktadır. Bu aletler tek kayma hızı ile çalışırlar. Akış eğrisi üzerinde tek bir nokta elde dilir, bu noktadan yapılan bir uzatma (ekstrapolasyon) ile tam bir akış eğrisi elde edilir. Newtonian olmayan akış sistemlerinin viskozitesinin tek noktalı prensibe göre çalışan aletlerle ölçülmesi yanlış sonuçlar verir; ancak, değişik hız gradyanlarında çalışılarak ölçüm yapmak mümkün olabilir. Bu tip sistemlerin reogramı çok noktalı viskometreler kullanılarak çizilmelidir. Viskometreler iki temel prensibe göre ölçüm yaparlar:1) Bir tüp içindeki sıvının akışa karşı direncini ölçmek, 2) sıvının içindeki katı cismin hareketine gösterdiği direnci ölçmek.

Saha ölçümlerine göre basınç dalgalanmaları güçlü bir şekilde manevra hızına, akışkan reolojisine, akışkan rejimine, kuyu geometrisine, dizinin açık veya kapalı durumda olmasına bağlıdır. Bu tezde, içteki dizinin eksenel hareketinden dolayı oluşan basınç dalgalanmalarını, dairesel diziyi dikdörtgene yakınlaştırarak saptamak için kararlı halde, kısmen analitik ve HBE akışkanları için yeni bir model sunulmuştur. Analitik çözüm lineer olmayan karmaşık denklemler içerir. Bu doğrusal olmayan denklemin çözümünde üs (n) 0.5 varsayılmıştır. Denklemi çözebilmek için HBE akışkanın hız profili üç farklı bölgeye ayrıldı. Her üç bölgeye sınır koşulları uygulanarak denklemler

çözüldü. Matematiksel türetmelerin sonucunda üç bilinmeyenli 3 farklı denklem elde edilmiştir. Bu bilinmeyenlerden iki tanesi hız profilinde denklemi çözebilmek için ayrılmış bölgenin uzaklıklarıdır. Diğer bilinmeyen ise basınç dalgalanmalarının hesaplamasında kullanılan sürtünme basınç gradyanıdır. Bu üç denklem Trust Region optimizasyon algoritması kullanılarak bir Python kodu ile çözülmüştür.

Son olarak, geliştirilmiş kısmen analitik yeni basınç dalgalanmaları modeli hem düzenli (ucu açık ve kapalı dizi) hem düzensiz kuyu geometrisine uygulanmıştır. İdeal olmayan Bingham plastik ve Herschel-Bulkley akışkanları ile kıyaslanarak sonuçlar doğrulanmıştır.

1. INTRODUCTION

Throughout drilling operations, the drillstring may be pulled out from the wellbore or run into the wellbore for different purposes for instance replacement of the bottomhole assembly or bit, etc. The drillstring can be removed or replaced by coupling up or emerging the tubulars that constructs the drillstring. This movement of the drillstring for a designated location is called as the tripping application. Pressure abnormalities is mostly produced due to tripping operations, or movement applied to the casing string during the cementing operations. The increase in pressure when pipe is run into the wellbore is termed as surge pressure. On the other hand, the decrease in pressure while pulling pipe is named as swab pressure.

Exact estimation of surge and swab pressures is important while evaluating the maximum tripping velocities to maintain the wellbore pressures within particular margins of pore and fracture pressures known as mud window. In many wells, drilling operations such as casing design or performing low clearance liner are conducted with using substantially wide pressure surges limits. Nevertheless, in critical wells such as deep offshore wells, highly deviated and horizontal wells, pressure surge margins must be narrow to inhibit fluid influx, lost circulation, blowout and kick. In these wells, a correct method or approach is required in order to predict pressure surges.

Managing time is more crucial than ever, as the drilling operations became more expensive compared to past practices. Therefore, drilling researches focused on determining surge and swab pressures accurately all the time. Since the oil and gas companies tend to drill unconventional complicated wells more, the understanding of precise surge pressure estimation in the wellbore provides a correct optimisation of drilling hydraulics and brings about more profitable drilling operations.

In this study, the general equations of the surge pressures with an exponential factor n=0.5, are analytically derived for Extended Herschel-Bulkley fluid model for steady, fully developed laminar flow in a narrow slot caused by axial movement of inner pipe. The analytical solution consists of treating a complex non-linear equations with an iterative procedure.

1.1 Rheology

Given enough time and force, all materials (solids, liquids and gases) eventually would flow. Rheology is the subject of how substances flow depending on relationship of shear rate and shear stress. The rheological properties of a substance may depend on pressure, temperature, and the rate and continuity of shear.

Rheological characterization is specifically critical for the oil and gas industry as the science of rheology investigate the flow behavior of fluids in pipes. Flow behavior can be classified as laminar and turbulent. In laminar flow, it is assumed that the concentrically placed drillstring in the casing or open hole, circular shaped open hole, stable drillstring, isothermal flow, and no slip at the walls of conduit. Laminar flow is valid at low velocities when flow is orderly, parallel to each other and without crossflow. If there is laminar flow regime, the fluid velocity at the edge of the pipe walls will be zero, and the fluid velocity increases by moving away from pipe walls until middle of the pipe where becomes maximum. In the real world, these assumptions are entirely incorrect. In nearly all drilling applications, the drilling fluid is pumped at too high rate for laminar flow to be maintained. Turbulent flow is valid at high velocities when flow is chaotic diffused flow pattern which requires empirical flow equations to describe.

In the oil field, petroleum engineers are generally concerned with shear stress which is the force per unit area required to sustain fluid flow. Shear stress is a function of the shear rate. Shear rate is rate at which the fluid velocity change with perpendicular to the direction of flow. The mathematical relationship between shear rate and shear stress is the rheological model of the fluid. Fluids can be classified as Newtonian and Non-Newtonian according to their rheological behavior. These rheological models are significant for the following applications in the oil industry:

- Computing the frictional pressure drop in pipes and annulus,
- Predicting the equivalent circulating fluid density (ECD),
- Characterizing the flow regimes in the annulus,
- Predicting surge and swab pressures,
- Predicting hole-cleaning efficiency,
- Well control,
- Bit optimization, and

- Improving the drilling performance.

1.1.1 Newtonian fluid model

The Newtonian model is developed from the simplest form of fluid flow behavior which has the linear constant fluid viscosity at constant temperature and pressure. Newtonian fluids begin to flow right away, and the shear stress increases with increasing shear rate. Many fluids, such as water, high gravity oils, alcohol and gasoline are example of fluids that shows Newtonian fluid behavior. Viscosity of the Newtonian fluids depends on only the fluid and its temperature. For Newtonian fluids, a plot of shear stress versus shear rate gives a straight line that begins from the origin as shown in Figure 1.1. Fluid flow does not have a consistent velocity through a pipe or a concentric annulus.

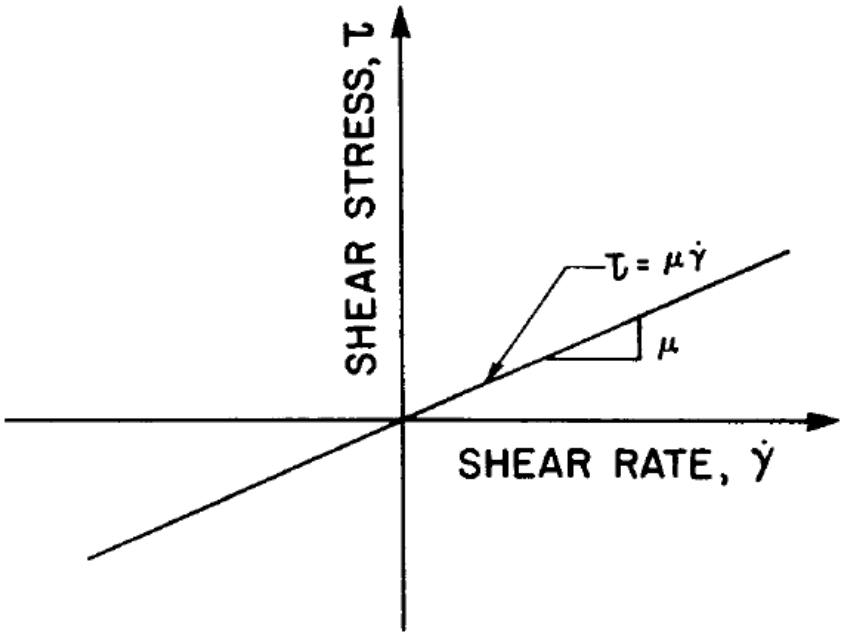

Figure 1.1: Newtonian fluid model behavior (Bourgoyne et al., 1991).

The Newtonian model states that the shear stress, τ [Pa], is directly proportional to the shear rate γ [s^{-1}]. And that behavior is expressed by equation below.

$$\tau = \mu\,\gamma \tag{1.1}$$

Frictional pressure loss equations for laminar and turbulent regime in pipe and annulus for Newtonian fluids are defined in Bourgoyne et al. (1991) with the following equations presented in Field units.

Pipe;

For laminar flow:

$$\frac{dp_f}{dL} = \frac{\mu\ \bar{v}}{1500\ d^2} \tag{1.2}$$

For turbulent flow:

$$\frac{dp_f}{dL} = \frac{\rho^{0.75}\bar{v}^{1.75}\mu^{0.25}}{1800\ d^{1.25}} \tag{1.3}$$

Annulus;

For laminar flow:

$$\frac{dp_f}{dL} = \frac{\mu\ \bar{v}}{1000\ (d_2 - d_1)^2} \tag{1.4}$$

For turbulent flow:

$$\frac{dp_f}{dL} = \frac{\rho^{0.75}\bar{v}^{1.75}\mu^{0.25}}{1396\ (d_2 - d_1)^{1.25}} \tag{1.5}$$

where

$\frac{dp_f}{dL}$ = Frictional pressure gradient, Psi/ft

ρ = Fluid density, lbm/gal

d = Internal pipe diameter, in.

μ = Fluid viscosity, cp

$\bar{v}$ = Mean flow velocity, ft/s

d_1 = Inside diameter of the inner pipe, in., and

d_2 = Outside diameter of the outer pipe, in.

1.1.2 Non-Newtonian fluid models

Most drilling fluids are too complicated to describe viscosity with a single parameter as they are composition of a lots of additives such as polymers. For these fluids classified as non-Newtonian, the rate of shear stress and shear rate does not give a constant proportion. Therefore, viscosity of non-Newtonian fluids changes with variation of shear rate. Non-Newtonian fluids are examined with different models. The most interested models in drilling engineering are the Bingham plastic, Power-law, Herschel-Bulkley (Yield Power Law) and Extended-Herschel-Bulkley models.

1.1.2.1 Bingham plastic model

The behavior of most water-based cement slurries can be characterized by the Bingham plastic model which accepts a linear relationship between the shear stress and the shear rate. Fluids that exhibit Bingham plastic behavior do not flow until the shear stress exceeds a critical value known as the yield point. Until yield point is reached, the shear stress is zero, and fluid behaves like solid under static conditions. Once the yield point is reached, changes in shear stress and shear rate are proportional. A graphical illustration of this behavior is shown in Figure 1.2. The slope of the plot is called as the plastic viscosity. The Bingham plastic model does not correctly estimate fluid flow behavior at low shear rates but it is convenient for continuous monitoring and treating of drilling fluids. The Bingham plastic model is described mathematically as follows:

$$\tau = \mu\,\gamma + \tau_y \tag{1.6}$$

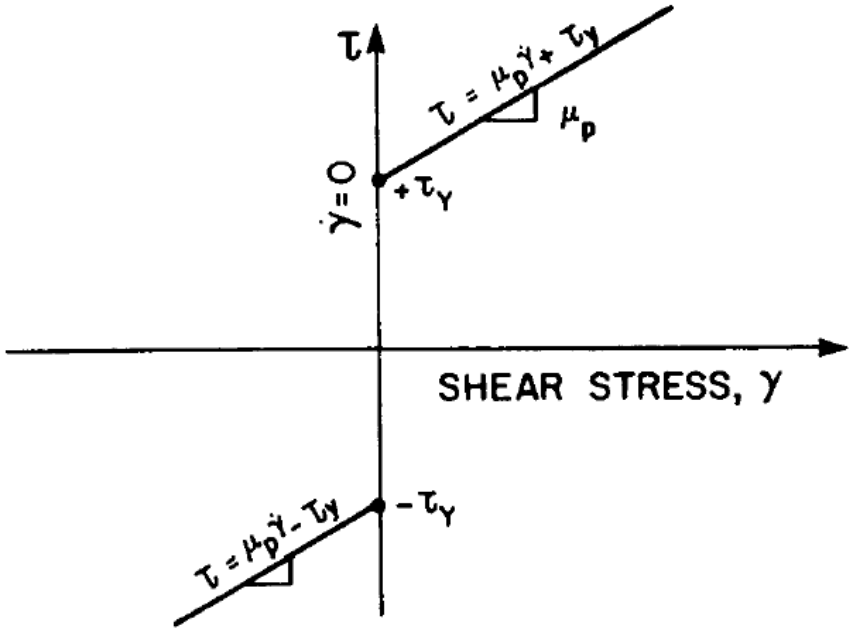

Figure 1.2: Bingham plastic fluid model behavior (Bourgoyne et al., 1991).

Frictional pressure loss equations for laminar and turbulent regime in pipe and annulus for Bingham plastic fluids are defined in Bourgoyne et al. (1991) with the following equations presented in Field units.

Pipe;

For laminar flow:

$$\frac{dp_f}{dL} = \frac{\mu_p\, \bar{v}}{1500\, d^2} + \frac{\tau_y}{225\, d} \tag{1.7}$$

For turbulent flow:

$$\frac{dp_f}{dL} = \frac{\rho^{0.75} \bar{v}^{1.75} \mu_p^{0.25}}{1800\, d^{1.25}} \tag{1.8}$$

Annulus;

For laminar flow:

$$\frac{dp_f}{dL} = \frac{\mu_p\, \bar{v}}{1000\ (d_2 - d_1)^2} + \frac{\tau_y}{200\ (d_2 - d_1)} \tag{1.9}$$

For turbulent flow:

$$\frac{dp_f}{dL} = \frac{\rho^{0.75} \bar{v}^{1.75} \mu_p^{0.25}}{1396\ (d_2 - d_1)^{1.25}} \tag{1.10}$$

where μ_p [cp] represents the fluid plastic viscosity and τ_y [$lb_f/100sq.ft$] represents the yield point as distinct from the pressure loss equations for Newtonian fluid model.

1.1.2.2 Power-law model

The Power-law model follow a non-linear relation between the shear stress and the shear rate. For Power-law fluids, the shear stress strengthens depending on the shear rate with a constant exponent. This model gives good results at low shear rates. There is no yield point for Power-law fluids. Thus Power-law fluids do not form gel strengths after force is stopped. Polymeric compounds behave as Power-law fluids. Power-law model can be used to represent a pseudoplastic fluid when exponent is less than 1, or a dilatant fluid when exponent is more than 1.

Pseudoplastic fluids exhibit a decreasing viscosity with an increasing shear rate shown in Figure 1.3a. This kind of behavior is termed as shear-thinning. Dilatant fluids is described by an increasing viscosity with an increasing shear rate shown in Figure 1.3b. This kind of fluids is called as shear-thickening liquids. The Power-law model is described mathematically as follows:

$$\tau = K\, \gamma^n \tag{1.11}$$

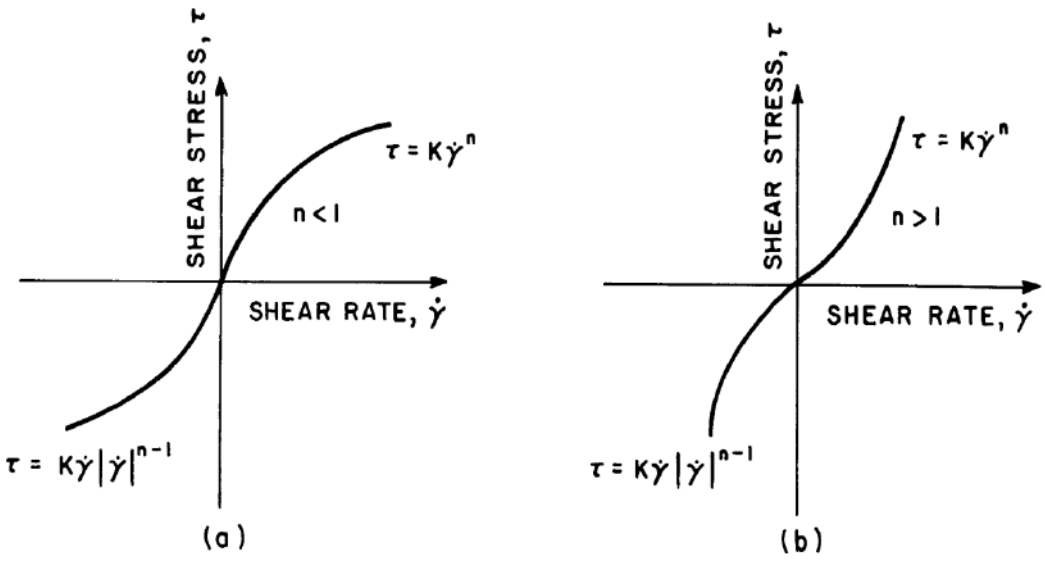

Figure 1.3: Power-law fluid model behavior (a) pseudoplastic fluid and (b) dilatant fluid (Bourgoyne et al., 1991).

Frictional pressure loss equations for laminar and turbulent regime in pipe and annulus for Power-law fluids are defined in Bourgoyne et al. (1991) with the following equations expressed in Field units.

Pipe;

For laminar flow:

$$\frac{dp_f}{dL} = \frac{K\,\bar{v}^n}{144000\,d^{1+n}}\left(\frac{3+1/n}{0.0416}\right)^n \tag{1.12}$$

For turbulent flow:

$$\frac{dp_f}{dL} = \frac{f\,\rho\,\bar{v}^2}{25.8\,d} \tag{1.13}$$

Annulus:

For laminar flow:

$$\frac{dp_f}{dL} = \frac{K\,\bar{v}^n}{144000\,(d_2-d_1)^{1+n}}\left(\frac{2+1/n}{0.0208}\right)^n \tag{1.14}$$

For turbulent flow:

$$\frac{dp_f}{dL} = \frac{f\,\rho\,\bar{v}^2}{21.1\,(d_2-d_1)} \tag{1.15}$$

where f represents the Fanning friction factor calculated from the Reynolds number, K $[lbf\text{-}s^n/100sq\ ft]$ is the consistency index of the fluid, and n is defined as the flow behavior index or the Power-law exponent.

1.1.2.3 Herschel-Bulkley model

Most fluids do not adjust exactly to a particular model but rather to a mixture of models. The Herschel-Bulkley model puts together the behavior of both Bingham plastic and Power-law model. The model is appropriate for fluids having a yield stress and a nonlinear relationship between the shear stress and the shear rate. Therefore, it precisely gives good results at high and low shear rates. Water-based and oil-based drilling fluids are example of fluids that exhibit Herschel-Bulkley behavior because both drilling fluid show shear-thinning behavior and have a yield stress.

A graphical representation of the Herschel-Bulkley model is demonstrated in Figure 1.4 by comparison with commonly used rheological models. The Herschel-Bulkley model is described mathematically as follows:

$$\tau = \tau_y + K\,\gamma^n \tag{1.16}$$

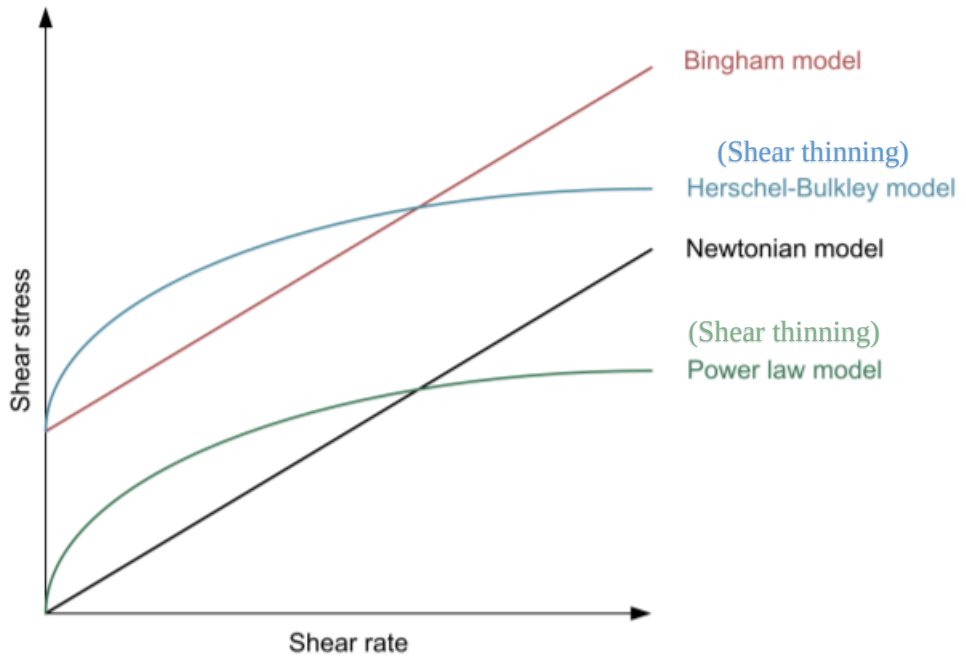

Figure 1.4: Herschel Bulkley fluid model behavior (Skalle, 2012).

The equation of Herschel-Bulkley model consists of three parameters that would represent the rheological behavior of fluids in the range of Bingham plastic and Power-

law models. The equation can be reduced to Bingham plastic model by substituting n=1 and K=μ_p. And Power-law model can be obtained by giving τ_y=0 into equation. Frictional pressure loss equations for laminar and turbulent flow regime in pipe and annulus for Herschel-Bulkley fluids are defined in Merlo et al. (1995) with following equations expressed in SI units.

Pipe;

For laminar flow:

$$\Delta p = \frac{2\,L\,K}{r}\left[\frac{\tau_o}{K} + \left[\left(\frac{3n+1}{n\,Cc}\right)\left(\frac{q}{\pi\,r^3}\right)\right]^n\right] \tag{1.17}$$

where,

$$q = \pi\,r^2 v_p \tag{1.18}$$

and,

$$Cc = 1 - \frac{1}{2n+1}\left\{\frac{\tau_0}{\tau_0 + k\left[\frac{(3n+1)q}{n\,\pi\,r^3}\right]^n}\right\} \tag{1.19}$$

for turbulent flow:

$$\Delta p = f\rho\frac{q^2}{\pi^2\,r^5}L \tag{1.20}$$

Since the friction factor is defined by:

$$f = y(Cc * Re)^{-z} \tag{1.21}$$

where,

$$Re = \frac{2\,\rho\,q}{\mu\,\pi\,r} \tag{1.22}$$

Apparent Newtonian viscosity in Eq.1.22 is defined by:

$$\mu = \frac{\tau_0 + k\left(\left(\frac{3n+1}{n\,Cc}\right)\left(\frac{q}{\pi\,r^3}\right)\right)^n}{\left(\frac{3n+1}{n\,Cc}\right)\left(\frac{q}{\pi\,r^3}\right)} \tag{1.23}$$

and,

$$y = \frac{\log(n) + 3.93}{50} \tag{1.24}$$

$$z = \frac{1.75 - \log(n)}{7} \tag{1.25}$$

Annulus:

For laminar flow:

$$\Delta p = \frac{2\,L\,K}{(r_2 - r_1)}\left[\frac{\tau_o}{K} + \left[\frac{2(2n+1)}{n\,Ca\,(r_2 - r_1)}\,\frac{q}{\pi\,({r_2}^2 - {r_1}^2)}\right]^n\right] \tag{1.26}$$

where,

$$Ca = 1 - \frac{1}{n+1}\left\{\frac{\tau_0}{\tau_0 + k\left[\left(\frac{2(2n+1)}{n\,(r_2 - r_1)}\right)\left(\frac{q}{\pi\,({r_2}^2 - {r_1}^2)}\right)\right]^n}\right\} \tag{1.27}$$

and,

$$q = \pi\,({r_2}^2 - {r_1}^2)v_a \tag{1.28}$$

For turbulent flow:

$$\Delta p = f\rho\frac{q^2}{\pi^2(r_2 - r_1)(r_2^2 - r_1^2)^2\,r^3}L \tag{1.29}$$

The friction factor in Equation 1.29 is defined by:

$$f = y(Ca * Re)^{-z} \tag{1.30}$$

where,

$$Re = \frac{2\,\rho\,q}{\mu\,\pi\,(r_1 + r_2)} \tag{1.31}$$

Apparent Newtonian viscosity in Equation 1.22 is defined by:

$$\mu = \frac{\tau_0 + k\left[\left(\frac{2(2n+1)}{n\,(r_2 - r_1)}\right)\left(\frac{q}{\pi\,Ca\,({r_2}^2 - {r_1}^2)}\right)\right]^n}{\left[\left(\frac{2(2n+1)}{n\,Ca\,(r_2 - r_1)}\right)\left(\frac{q}{\pi\,({r_2}^2 - {r_1}^2)}\right)\right]^n} \tag{1.32}$$

and,

$$y = \frac{\log(n) + 3.93}{50} \tag{1.33}$$

$$z = \frac{1.75 - \log(n)}{7} \tag{1.34}$$

where

Cc = Correction coefficient for the pipe

Ca = Correction coefficient for the annulus

Δp = Pressure drop, Pa

q = Flow rate, m^3/s

r_1 = Inner radius of annulus, m

r_2 = Outer radius of annulus, m

r = Inside drill pipe annulus, m

L = Measured length, m

Determination of correction coefficients for the pipe and for the annulus and the Fanning friction factor corresponding to these coefficients can be found in detail in the study by Merlo et al. (1995).

1.1.2.4 Extended Herschel-Bulkley model

The Extended Herschel-Bulkley (HBE) model combines the effects of Bingham plastic, Power-law and Herschel-Bulkley behavior in a fluid. Even though Herschel-Bulkley model gives good results for most drilling fluid, some rheological behavior of fluids cannot be characterized by the Herschel-Bulkley model. At the very high shear rate, apparent viscosity becomes constant in the large range. Madlener et al. (2009) demonstrated the Extended Herschel-Bulkley equation by adding an external term to Herschel Bulkley model for better explanation of viscosity behavior. The Extended Herschel-Bulkley model is described mathematically as follows:

$$\tau = \tau_y + K\,\gamma^n + \mu_\infty \gamma \tag{1.35}$$

where μ_∞ represents the constant or equilibrium viscosity at the wide shear rate range. An example of that behavior comparing to Power-law model is illustrated in Figure 1.5. Legends of Figure 1.5 are fixed since it is wrong in published article. As the Power-law model is unable to characterize the viscosity behavior of the fluids surveyed on the complete shear-rate range, Reynolds number based on Power-law model cannot be applied to describe the fluid flow. Madlener et al. (2009) developed a generalized Extended Herschel Bulkley Reynolds number to explain that behavior of such fluids.

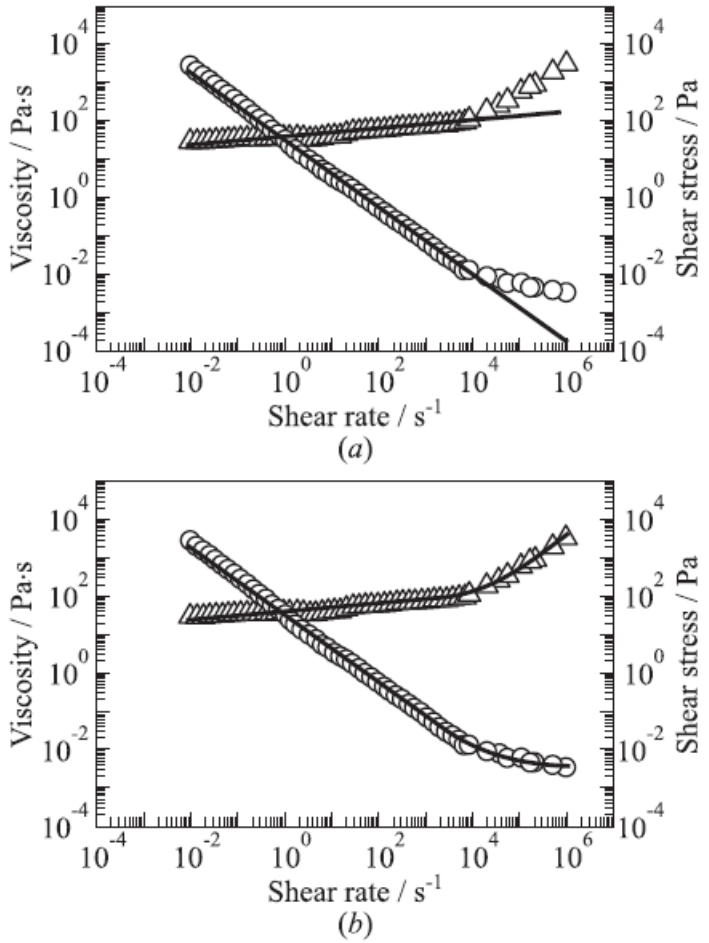

Figure 1.5: Viscosity evaluation of a kerosene with rheological approach (a) PL and (b) HBE: Δ – shear stress and O – viscosity (Madlener et al, 2009).

Metzner and Reed (1955) presented a generalized Reynolds number associated with the Darcy friction factor. This relationship is expressed by the following equation.

$$Re = \frac{64}{f_{darcy}} \tag{1.36}$$

Note that, in this equation Moody friction factor is used. For Fanning friction factor, it is defined as $f_{Moody} = 4\, f_{Fanning}$ where the Darcy friction factor equals to

$$f_{darcy} = \frac{\left(-\frac{\Delta p}{L}\right) D}{\rho\, \bar{v}^2} \tag{1.37}$$

where Δp means the pressure loss through the pipe length L and the pipe diameter D, and $\bar{v}$ represents the mean velocity of flow. The relationship of the pressure drop with shear stress at the wall τ_w is computed from the force balance on the pipe with

$$\tau_w = \frac{D\Delta p}{4L} \tag{1.38}$$

For Newtonian fluids, shear stress at wall can be defined by

$$\tau_w = \mu\gamma_w \tag{1.39}$$

where μ is called as the Newtonian viscosity and γ_w represents the shear rate at the wall. In pipe flow, the shear rate is expressed by

$$\gamma_w = \frac{8\,\bar{v}}{D} \tag{1.40}$$

when the friction factor equation is rewritten in terms of the definitions of shear rate and shear stress, Eq. 1.37 becomes

$$f_{darcy} = \frac{64\,\mu}{\rho\,\bar{v}\,D} \tag{1.41}$$

For non-Newtonian fluid, the shear stress τ_w must be computed using the viscosity of the Extended Herschel-Bulkley-type. As the shear rate is described as the negative velocity gradient, Extended Herschel-Bulkley model can be written as:

$$\tau_w = \tau_o + K\left(-\frac{dv}{dr}\right)_w^n + \mu_\infty\left(-\frac{dv}{dr}\right)_w \tag{1.42}$$

Rabinowitsch (1929) and Mooney (1931) derived a definition for the shear rate for Newtonian fluids which can be applied also to non- Newtonian fluids.

$$\left(-\frac{dv}{dr}\right)_w = \frac{3}{4}\left(\frac{8\bar{v}}{D}\right) + \frac{1}{4}\left(\frac{8\bar{v}}{D}\right)\frac{d\left(\ln\left(\frac{8\bar{v}}{D}\right)\right)}{d\left(ln\left(\frac{D\Delta p}{4L}\right)\right)} \tag{1.43}$$

The logarithmic part of equation above can be rewritten in terms of local gradient m which corresponds to the rate of the shear stress τ_w to apparent shear rate $\gamma_{app,w}$ since unlike Power-law fluid, the local gradient m may vary with exponent n for Extended Herschel-Bulkley fluid.

$$\frac{d\left(\ln\left(\frac{8\bar{v}}{D}\right)\right)}{d\left(ln\left(\frac{D\Delta p}{4L}\right)\right)} = \frac{d\left(ln(\gamma_{app,w})\right)}{d(ln(\tau_w))} = \frac{1}{m} \tag{1.44}$$

Then shear rate equation becomes

$$\left(-\frac{dv}{dr}\right)_w = \frac{3m+1}{4m}\left(\frac{8\bar{v}}{D}\right) \tag{1.45}$$

Inserting Eqs. (1.42) and (1.45) into the friction factor equation yields:

$$f_{darcy} = 8\left(\tau_o + K\left(\frac{3m+1}{4m}\right)^n\left(\frac{8\bar{v}}{D}\right)^n + \mu_\infty \frac{3m+1}{4m}\left(\frac{8\bar{v}}{D}\right)\right)\Big/(\rho\,\bar{v}^2)$$

$$= \frac{64\left(\frac{\tau_o}{8} + \left(\frac{D}{\bar{v}}\right)^n + K\left(\frac{3m+1}{4m}\right)^n 8^{n-1} + \mu_\infty \frac{3m+1}{4m}\left(\frac{D}{\bar{v}}\right)^{n-1}\right)}{(\rho\,\bar{v}^{2-n}\,D^n)} \tag{1.46}$$

The generalized Reynolds number for the extended Herschel-Bulkley equation is defined by replacing the friction factor from Eq. 1.46 into Eq. 1.36:

$$Re_{HBE} = \frac{(\rho\,\bar{v}^{2-n}\,D^n)}{\left(\frac{\tau_o}{8} + \left(\frac{D}{\bar{v}}\right)^n + K\left(\frac{3m+1}{4m}\right)^n 8^{n-1} + \mu_\infty \frac{3m+1}{4m}\left(\frac{D}{\bar{v}}\right)^{n-1}\right)} \tag{1.47}$$

where

$$m = \frac{n\,K\,(8\bar{v}/D)^n + \mu_\infty(8\bar{v}/D)}{\tau_o + K\,(8\bar{v}/D)^n + \mu_\infty(8\bar{v}/D)} \tag{1.48}$$

The local gradient is solved by differentiation of the logarithmic term displayed below:

$$m = \frac{d\left(ln(\tau_w)\right)}{d\left(ln(\gamma_{app,w})\right)} = \frac{d\left(ln\left(\tau_o + K\,\gamma_{app,w}^n + \mu_\infty\gamma_{app,w}\right)\right)}{d\left(ln(\gamma_{app,w})\right)} \tag{1.49}$$

The equation of Extended Herschel-Bulkley model consists of four parameters make available to convert the rheological behavior of fluids to Herschel-Bulkley, Bingham plastic, Power-law or Newtonian models. The generalized Reynolds number equation of Extended Herschel-Bulkley fluids can be reduced to Herschel-Bulkley model by replacing μ_∞=0. Bingham plastic model by substituting μ_∞= μ_p, n=1 and K=0. And Power-law model can be obtained by giving μ_∞=0 and τ_y=0 into equation.

1.2 Surge and Swab Models

1.2.1 Steady state models

Steady state surge models are mostly used while evaluating pressure surges in critical wells such as those introduced by Burkhardt (1961), Schuh (1964), and Fontenot and

Clark (1974). The pipe movement completely removes the drilling mud in these models. Fluid pressures are computed with respect to non-Newtonian frictional pressure drops because of this fluid action. These models do not take into account effect of fluid inertia (Inertia effect is roughly involved in Burkhardt's model), the fluid compressibility, and the pipe elasticity. The absence of fluid compressibility is relatively safe assumption because it estimates a greater flow rate which brings about a greater frictional pressure drop. Neglecting fluid inertia is a risky assumption because, as an example, negative surge pressures may observed as a result of fluid backflow during the pipe motion is stopped. Assuming rigid pipe displacement is conservative because considering axial elasticity of the pipe makes the rate of fluid displacement less.

Burkhardt (1961) developed the concept of pressure surges originated from viscous drag by simplified charts and computation methods to be applicable in field operations. He emphasized that all single peak pressures in the surge pattern which is shown in Figure 1.6 may arise from viscous drag, fluid inertia and mud gel breaking.

He mentioned the gel breaking effect is valid only if the pressure is insufficient to break the gel and the pipe is stopped. Whenever these conditions are not provided, pressure surges must be stemmed from fluid inertia and viscous drag. He also stated that the surge pressures stemming from inertial effect is based on the mud column resisting a shift in motion. Predicting pressure surges stemming from viscous drag is theoretically more complicated.

Burkhardt (1961) investigated a method to calculate surge pressures is due to the viscous drag forces as a result of pipe motion. The axial mean velocity is considered in hydraulic calculations. The velocity caused by mud volume created by the displacing pipe (V_{da}) and the average effective velocity (V_{ae}) in the annular flow are expressed by the following equations;

$$V_{da} = -\left(\frac{D_p^2}{D_h^2 - D_p^2}\right) V_p \tag{1.50}$$

$$V_{ae} = -\left(\frac{D_p^2}{D_h^2 - D_p^2} + K\right) V_p \tag{1.51}$$

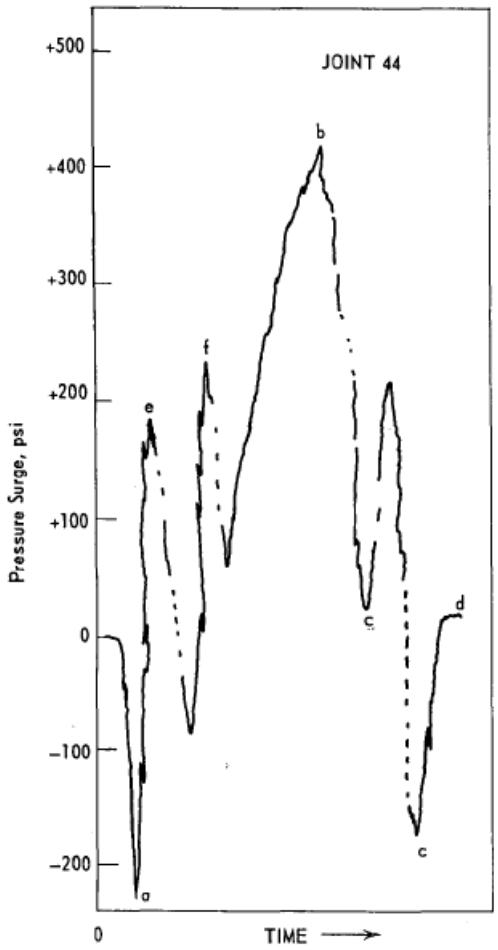

Figure 1.6: An example of pressure surge pattern (Burkhardt, 1961).

where the pipe diameter is presented by D_p and the hole diameter is termed as D_h and the pipe velocity is given by V_p. K is the mud clinging constant that can be acquired from a chart established by Burkhardt (1961) which is shown in Figure 1.7.

A dimensionless quantity named as Bingham number or plasticity (S), and conductance (ω) characterized by Melrose (1958) were used to identify the flow regime and determine the friction factor. The plasticity and conductance numbers are expressed as below:

$$S = 2394\frac{\left(D_h - D_p\right)\tau_o}{\mu_p V_{ae}} \tag{1.52}$$

$$\omega = 1 - \frac{\omega\, S}{8} + \frac{1}{2}\left(\frac{\omega\, S}{12}\right)^4 \tag{1.53}$$

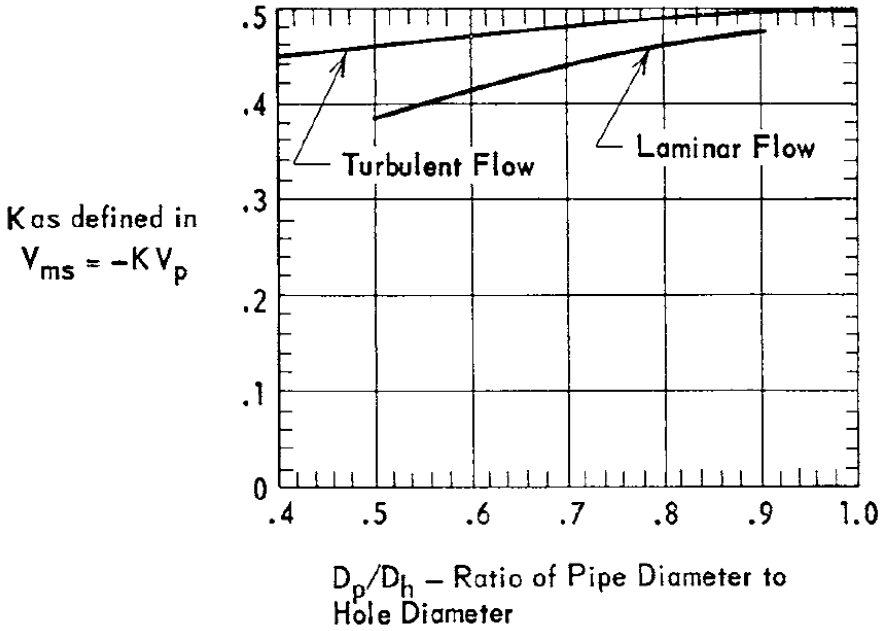

Figure 1.7: Mud clinging constant (Burkhardt, 1961).

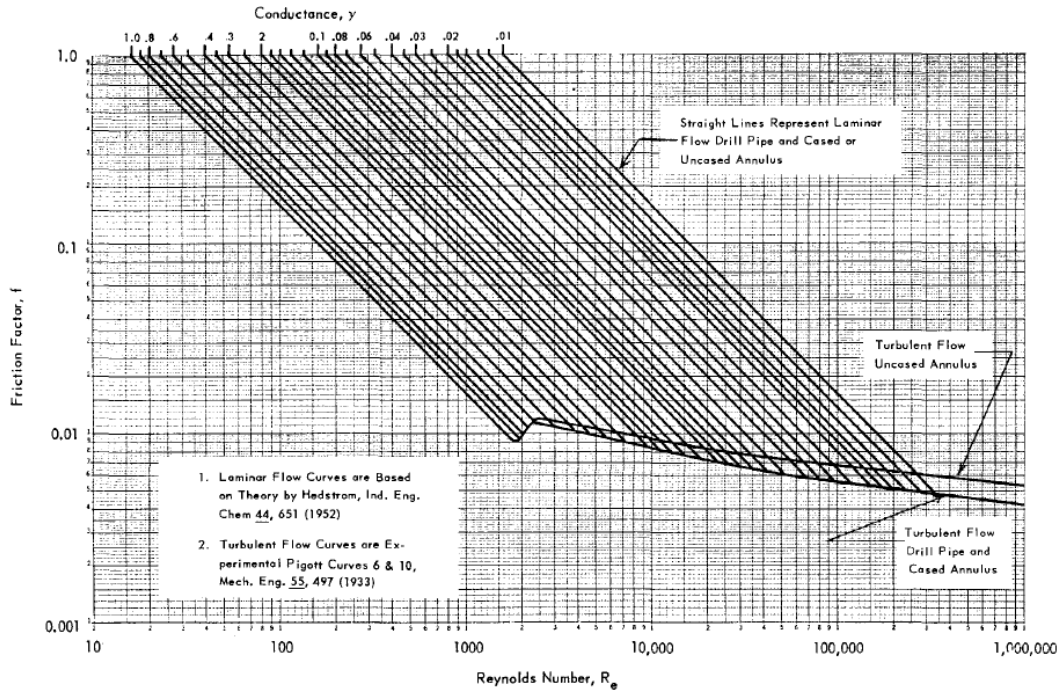

Figure 1.8: Modified friction factor vs Reynolds number chart (Burkhardt, 1961).

Burkhardt (1961) developed an improved friction factor-Reynolds number chart for Bingham plastic fluids. The Reynolds number equation was expressed by,

$$R_e = 15.44 \frac{(D_h - D_p)B_{ae}\rho}{\mu_p} \tag{1.54}$$

In order to find modified friction factor, Burkhardt (1960) presented a chart associated with the Reynolds number and conductance which is displayed in Figure 1.8.

He defined the pressure surge produced by the average effective mean velocity in the annulus due to closed-pipe motion in the borehole with the following equation:

$$\frac{\Delta P}{\Delta L} = \frac{f_b V_{ae}^2 \rho}{9.282 \times 10^4 \left(D_h - D_p\right)} \tag{1.55}$$

1.2.2 Unsteady state (dynamic) models

A dynamic model estimates surge and swab pressures more correctly than a steady-state model by determining better prediction of fluctuations in pressure while pipe is tripped. In 1977, Lubinski, et al., established the first unsteady state model. This attempt was advanced by Lal (1983), still both these models are considered that the moving pipe conducted as a rigid body. Mitchell (1988) included axial pipe elasticity to dynamic surge interpretation. Bing et al. (1995) showed some inadequacies in reports of Lubinski et al. (1977), Lal (1983), and Mitchell (1988). The dynamic models accurately predict maximum surge and swab pressures in conjunction with variation of pressure with time at any position in the well bore. Estimating surge and swab pressures using dynamic models can reduce promising problems in a well bore and provide more profitable trip speeds for running or pulling pipe.

Mitchell (1988) developed a dynamic surge/swab model that enhanced current science along with some traits such as coupled pipe and annulus pressures by way of the pipe elasticity, pipe displacement determination through lengthwise pipe elasticity and viscous drag forces, changeable fluid properties as a function of pressure and temperature, and employing pipe elasticity, formation elasticity, and cement elasticity to complete the complex elastic return of the wellbore.

Mitchell's dynamic surge/swab pressure model is one of the most approved among the established models. The model also considers the temperature affecting fluid rheology, fluid circulation, inclined wells, acceleration and eccentricity. Nevertheless, he did not show the exact formulation of the model in his paper.

He presented two analytical models illustrated in Figure 1.9 made up of the coupled-pipe/annulus model and the pipe-to-bottomhole model in his paper. The fluid-flow part of the coupled-pipe/annulus model and the pipe-to-bottomhole model are determined

by using the interpolation method of aspects. He explained the elastic pipe movement by employing the finite elements method in order to find out the pipe equations. He applied tridiagonal algorithm to resolve the equations for the trip speed. He determined the fluid movement and pipe speed equations based on the boundary conditions and Newton Raphson's method is applied to figure out the equations in consideration of nonlinear boundary conditions.

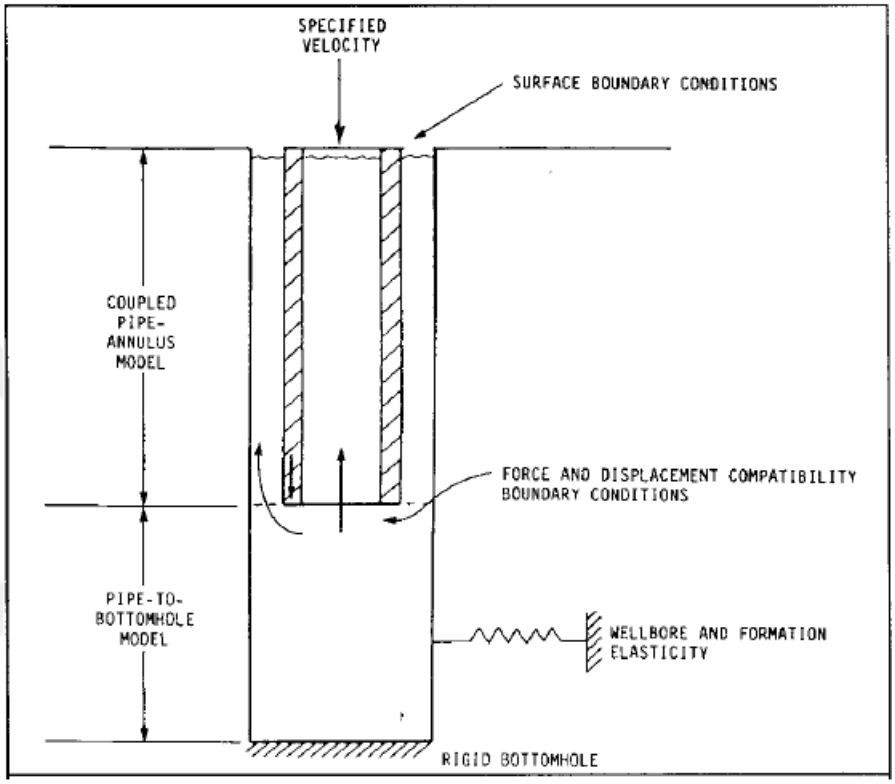

Figure 1.9: Illustration of model flow regimes (Mitchell, 1988).

Pipe-to-Bottomhole Model: The open hole below the drill pipe is considered in pipe-to-bottomhole model. Two partial-differential equations which are based on the balance of mass and the balance of momentum are used in order to obtain the fluid pressures and velocities.

Mass Balance Equation:

$$\left|\frac{1}{A}\frac{dA}{dp}+\frac{1}{K}\right|\frac{dp}{dt}+\frac{\partial v}{\partial z}=0 \tag{1.56}$$

The balance of mass is expressed by three terms: The expansion of the hole caused by internal fluid pressure, dA/dp, the compression of the fluid for the reason that changes in fluid pressure. The expansion of the hole is conducted by the elastic reaction of the formation and casing between the formation and the fluid. The fluid volume difference

is produced by the bulk modulus, K., K depends on pressure, temperature, and composition of drilling muds. The reverse of the bulk modulus is termed as the compressibility.

Momentum Balance Equation:

$$\rho \frac{dv}{dt} = -\frac{\partial p}{\partial z} + \Delta p(v) + \rho g \, cos\theta \tag{1.57}$$

The momentum balance equation are formed from four terms. The first term in Eq. 1.57 describes the inertia of the fluid. The terms in the right side of Eq. 1.57 are the forces applied to fluid which are respectively the pressure gradient, the drag frictional or viscous forces, and the gravitational force. The drag is given by the function Δp depends on the fluid type and fluid velocity.

Coupled-Pipe/Annulus Model: The pressures and flow speeds in the pipe and annulus are formed by partial differential equations which are based on mass balance equations and momentum balance equations for both pipe and annulus.

Pipe-Flow Balance of Mass:

$$\left|\frac{1}{A_1}\frac{dA_1}{dp_1} + \frac{1}{K_1}\right|\frac{dp_1}{dt} + \left|\frac{1}{A_1}\frac{dA_1}{dp_2}\right|\frac{dp_2}{dt} + \frac{\partial v_1}{\partial z} = 0 \tag{1.58}$$

Pipe-Flow Balance of Momentum:

$$\rho_1 \frac{dv_1}{dt} = -\frac{\partial p_1}{\partial z} + \Delta p(v_1 - v_3) + \rho_1 g \, cos\theta \tag{1.59}$$

Annulus-Flow Balance of Mass:

$$\left|\frac{1}{A_2}\frac{dA_2}{dp_1}\right|\frac{dp_1}{dt} + \left|\frac{1}{A_2}\frac{dA_2}{dp_2} + \frac{1}{K_2}\right|\frac{dp_2}{dt} + \frac{\partial v_2}{\partial z} = 0 \tag{1.60}$$

Annulus-Flow Balance of Momentum:

$$\rho_2 \frac{dv_2}{dt} = -\frac{\partial p_2}{\partial z} + \Delta p_2(v_2, v_3) + \rho_2 g \, cos\theta \tag{1.61}$$

There are two substantial differences between these balance equations and the equations for the pipe-to-bottomhole model. First, the expansivity of mass balance equations rely on the pressures both inside and outside the pipe. For instance, raised annulus pressure can reduce the cross-sectional area within pipe and increase in pipe pressure can expand the cross-sectional area in consequence of pipe elastic

deformation. The second important difference is the effect of pipe velocity on the frictional pressure drop through the annulus. Finally the pipe/annulus model is the pipe balance of momentum is described below.

Elastic Pipe Balance of Momentum:

$$\rho_3 \frac{d^2 v_3}{dt^2} = E \frac{\partial v_3}{\partial z^2} + f_1 \frac{\partial}{\partial z^2} \frac{dp_1}{dt} + f_2 \frac{\partial}{\partial z} \frac{dp_2}{dt} + f_3 \frac{dv_1}{dt} + f_4 \frac{dv_2}{dt} + f_5 \frac{dv_3}{dt} \quad (1.62)$$

In the improvement of the surge pressure model, inertia effect, the left side of Eq. 1.62, was ignored. On the other side, the first term in Eq. 1.62 is Young's modulus, E with the longitudinal elasticity of the pipe. The second and third terms maintain the hoop-stress effect. For example, increasing the inner pressure shortens the pipe length and increasing outside pressure elongates the pipe length. And other terms define fluid viscous drag on the pipe.

2. LITERATURE REVIEW

In the early part of twentieth century, increasing number of blowouts lead people to research the reason behind that. According to research conducted, most blowouts in the history has been connected to surge and swab. First study of surge and swab were put into practice by Cannon in 1934 as a potential reason for pressure change while withdrawing drillpipe from the hole. He stated that withdrawing pipe decreases the mud pressure and it causes decline in hydrostatic pressure. If the amount of this reduction is enormous, formation pressure can be more than hydrostatic pressure and results in blowouts. He demonstrated that fluid influx and blowouts are associated with excessive swab pressures which are essentially depend on gel strength, viscosity of mud, the length of pipe in the hole, rate of withdrawal and the size of the annulus. The report of Cannon only involves swabbing pressure and about pressure surge is never talked.

Later, Horn (1950) and Goins et al. (1951) studied measurement of surge pressures in different situation in order to determine effects of running and withdrawing pipe. Based on the consequences of these studies, surge pressure increased with depth and faster rate of pipe movement. Goins and his associates indicated that surge pressures have greater effect than swab pressure. Therefore, they investigated only surge pressures.

In 1953 Cardwell explained that Cannon (1934) and Goins et al. (1951) worked on same subject but in different directions. However their reports were different in the measure of effects which are connected to pressure change such as gel strength, viscosity, and rate of pipe. Cardwell (1953) and Ormsby (1954) showed that magnitude of the pressure change in both direction should be the same. Cardwell attributed the inconsistency to use of different kind of fluids and slower rate of pulling the pipe than running. Also they made use of standard pressure-drop equations in laminar and turbulent regime to correlate calculated and measured reading for Newtonian fluid. However, they both considered pressure drops stemming from the viscous drag of the moving mud with stationary pipe wall.

Clark (1956) published idealized graphs of surge pressures and developed equations in order to infer surge pressures in a concentric annulus for Bingham Plastic fluid. His approach was more complete than theories of Cardwell (1953) and Ormsby (1954) because he mentioned pressure change arising from inertial effects in addition to their reports. However, he did not mention effects of gel strength in pressure change. Moreover, use of his equations were not favorable in the field because they were too complicated.

All these theories was not compared with measured surge pressures. Burkhardt (1961) developed a semi-empirical method measuring surge pressures produced by pipe movement in a mud-filled wellbore and compared that quantitative and theoretical model by experimentation for Bingham Plastic fluid. He accurately predicted the magnitude of pressures generated by breaking the mud gel, inertia and viscous drag of the mud column. He concluded that surge pressures are usually high because of viscous drag when running the drill pipe or casing without fill-up tools.

Schuh (1964) improved Burkhardt's (1961) numerical model to compute surge and swab pressure for Power-law fluids in concentric annuli at steady state flow. He developed a computer program to find bottom hole pressure arising from surge. And he used parameters consisted of yield point, viscosity, density of drilling mud, gel strength, annular geometry and tripping speed in his equations. By changing parameters, he tried to analyze the effects of these parameters when the pipe is run either closed or open-ended.

Fontenot and Clark (1974) improved equations developed by Burkhardt (1961) and Schuh (1964) to calculate downhole pressures resulting from fluid circulation and drillstring movement in steady-state flow in a cylindrical pipe and a stationary concentric cylindrical annulus. They programmed equations as a computer solution for Bingham Plastic model which can be converted to Power-law model by entering constants to calculate circulating pressure losses and surge/swab pressures in the wellbore. When the mud flow rates and pipe speeds are entered, circulation pressure and surge/swab pressure are calculated respectively in their computer program. The method gives good results compared to field measurements and it is important that drilling fluid properties in various depths can be observed in the method.

All these models assumed steady-state flow but in fact it is unsteady state flow as pipe is moving. Lal (1983) presented a dynamic surge and swab models using physics of

the transient phenomena for Power-law fluid. He developed a computer program which can estimate maximum surge and swab pressures and calculate the safe trip velocity for a specified pressure margin or effective circulating density. The computer program considers various parameters in complex hole geometry, borehole expansion, varying trip speed and the properties of the mud to see their effects on surge and swab pressures. It also warns danger in case of lost circulation or kick. He compared his results with results of Burkhardt (1961) and showed the effect of unsteady state model.

Mitchell (1988) developed a dynamic surge model consists of coupled-pipe/annulus and pipe to bottomhole in laminar flow for Power-law fluid. He improved surge/swab model by determining pipe elasticity, pipe displacement and fluid properties depending on pressure and temperature. He used field data taken from Burkhardt (1961) and Clark and Fontenot's (1974) papers and converted his model to steady state to compare the results thereby showing the importance of dynamic model. He concluded that dynamic model gives better results than steady state model while predicting negative surge pressure and peak surge pressures. Also, he stated that inertial forces and friction forces gain importance in shallow wells on the other hand, fluid compressibility has more effect in deeper wells.

Bing et al. (1995) analyzed the surge and swab pressures for Herschel Bulkley fluids in an eccentric annuli due to clinging power throughout tripping. They tested their dynamic model and published steady-state models in the oil field. They concluded that the steady state surge and swab models may predict considerable errors in deeper wells, on the other hand their dynamic model showed a good agreement with the analysis of surge and swab pressures taken from the tested field. Tested data also showed that the surge and swab pressures are lower in an eccentric annulus in comparison with in a concentric annulus.

Early studies on surge and swab pressures assumed that a concentric annular geometry. Yang and Chukwu (1995) analyzed the steady laminar Couette flow of non-Newtonian Power-law fluids in a narrow eccentric annulus to determine the surge and swab pressures. They stated that analytical solution of that model gives the solution in a nondimensional and less complex form. They presented the graph for varying pipe/borehole eccentricity ratios and flow behavior indices of drilling fluids. Maximum pipe velocity is found with the aid of that graph. According to their results,

surge pressures decrease with increasing fractional eccentricities. Further they approved that surge and swab pressures are over estimated in concentric annuli.

Dynamic couette flow model has never studied to solve surge and swab pressure equations in concentric cylinder motion in the previous reports. Wang and Chukwu (1997) published analytical solution of surge and swab equations in unsteady state flow for non-Newtonian Power-law fluids. They used perturbation method to solve motion equations analytically. As the equations are in the form of dimensionless and graphical for different geometries and Power-law fluid index, it is simple to compute the surge and swab pressure for an unsteady motion of pipe movement in a concentric annuli. It is concluded from the results obtained from data analysis that surge and swab pressure gradient increases with increasing pipe acceleration and pipe/hole diameter ratio. However they assumed that the perturbation parameter is much smaller than unity. Therefore, their study gives correct results only if the annular gap is very small but not accurate at high eccentricities.

Hussain and Sharif (2009) numerically solved the surge and swab pressures for axial laminar flow of viscoplastic Yield Power-law (Herschel-Bulkley) fluids in a closed end eccentric annuli by reason of axial movement of the inner pipe. They coded solution employing a second-order finite-difference scheme giving reason for an exponential model in the interest of the shear stress to discretize the governing equation. They analyzed how pressure gradient is affected by generalized Bingham number, eccentricity, Power-law fluid index, and blockage height. There has not been any data in eccentric annuli to compare their numerical results. Therefore, they confirmed the results approaching analytical solution in a concentric annuli. They found out that the pressure gradient decreases if the eccentricity and blockage height increase and surge and swab pressure is proportional to the generalized Bingham number and flow behavior index.

Crespo et al. (2012) published a new analytical solution for narrow slot geometry to compute surge and swab pressures at steady state laminar flow in concentric annuli for Herschel-Bulkley fluid. After using the conservation equations and employing the flow boundary conditions, their analytical solution gives a nonlinear equation. Numerical method is applied to simplify nonlinear equation to exact equation by using different pressure gradient. Then, an analytical model which can be adjusted to other previous models is developed with dimensionless analysis techniques. Surge and swab

pressures of this model show good agreement in comparison with the results of Burkhardt (1961), Schuh (1964), Fontenot and Clark (1974). Based on their study, they resulted in surge and swab pressures are considerably influenced by yield stress, pipe velocity and diameter ratio. The effect of pipe velocity decreases for fluids having high yield stress. Crespo and Ahmed improved their reports with laboratory experiments analyzing the impacts of fluid properties, pipe speed and borehole geometry on surge and swab pressures. Based on the experiments, surge and swab pressures are reduced (up to 45%) with increasing pipe eccentricity.

Erge et al. (2018) numerically and analytically developed a surge and swab pressure model in concentric annuli for Yield Power-law fluids. In analytical model, conservation of momentum and boundary conditions are employed to solve equation. As surge and swab pressures for Yield Power-law fluids are nonlinear equation, they presented a numerical model arising from equation of moving pipe. They analyzed the results by using computational fluid dynamics software. Their model considers the effect of declination in annular geometries. Based on the study, they concluded that surge and swab pressures increase with increasing the diameter ratio and the pressure become more significant for narrow annulus. Moreover, they showed that surge and swab pressures increase with decreasing the shear thinning attribute of the fluid.

Recently, Ettehadi and Altun (2018) developed a semi analytical model in a slot geometry for Herschel Bulkley fluid to compute surge pressures arising from pipe motion. They used both high temperature high pressure rheometer and rotational viscometer to calculate pressure surges at different temperatures. Hereby, they observed that use of conventional viscometer causes wrong prediction of surge pressures. As their analytical solution of model can be converted for Power-law and Bingham Plastic model, they easily validated the results by comparison of existing models. They also considered fluid circulation case which is fixed boundaries to derive pressure loss equation in pipe for Herschel Bulkley fluid by eliminating pipe velocity terms. In the light of the pressure surge results obtained from their model, they detected good matches with well accepted published models. As distinct from previous existing models, they investigated that maximum pipe speed can be more than speed obtained from mud properties which is measured with conventional viscometer.

3. PURPOSE OF THE STUDY

As what mentioned in the first chapter, surge and swab pressure calculations are very significant for the safety and minimizing the drilling costs. Rheological model selection has a important role in determining the surge and swab pressures accurately. Since there is not any research conducted predicting surge and swab pressures using Extended Herschel-Bulkley (HBE) model in the literature, this study focuses on HBE model.

Firstly, in this study, developing analytical equations for a HBE fluid is aimed to calculate surge and swab pressures stemming from the movement of drillstring in a borehole assuming laminar flow regime and slot geometry.

In the second place, to validate the results, developed equations for a HBE fluid are applied to two cases in a wellbore geometry which are uniform (open-ended and closed-ended) and non-uniform geometry by comparing with the other types of non-Newtonian fluids, particularly for Bingham plastic and Herschel-Bulkley.

4. MODEL DERIVATION FOR HBE FLUID

Following assumptions are made in developing model through in this study:

- Drilling mud is a single phase, viscous and non-Newtonian fluid.
- Drillstring and annulus are fully filled by drilling fluid.
- Flow regime is laminar and steady state (fully developed flow).
- Constant drillstring velocity.
- The drillstring is assumed to be open-ended through to bit nozzles; therefore, the inertial effect is small and ignorable (Bourgoyne et al., 1991).
- The drillstring is concentric in the wellbore.
- No slip conditions at the walls and no borehole expansion.
- Incompressible fluid (density of the fluid is constant).
- Axial flow under isothermal conditions.
- Flow behavior index (n) is equal to 0.5.

The mathematical derivations of the newly proposed model are detailed in Appendix A. First the shear stress relationships are developed by integrating Equation A.1.9 over specific boundary condition for inner (Region I) and outer (Region III) layers. The velocity profile of each region is obtained from Equation A.1.9 and shear stress relationship for corresponding region. Then the flow rate is determined by integrating the velocity profile over the area for each region. At the end of mathematical derivation three equations for frictional pressure loss (FPL) due to drillstring movement are obtained as following:

$$\frac{dP_f}{dL} - \frac{2\tau_y}{h(\lambda_2 - \lambda_1)} = 0 \tag{4.1}$$

$$\begin{aligned} &-\frac{\lambda_1 h}{2\alpha^2} - \frac{\beta(\lambda_1 h)^2}{2\alpha} - \frac{1}{12\alpha^3\beta} + \frac{[1+4\alpha\beta(\lambda_1 h)]^{\frac{3}{2}}}{12\alpha^3\beta} - \frac{(\lambda_2 h)}{2\alpha^2} + \frac{\beta(\lambda_2 h)^2}{\alpha} \\ &+\frac{1}{12\alpha^3\beta} + \frac{h}{2\alpha^2} + \frac{\beta h^2}{2\alpha} - \frac{\beta(\lambda_2 h^2)}{\alpha} - \frac{[1+4\alpha\beta(h-\lambda_2 h)]^{\frac{3}{2}}}{12\alpha^3\beta} - v_p = 0 \end{aligned} \tag{4.2}$$

$$\left\{\left[\frac{(\lambda_1 h)^2}{4\alpha^2}-\frac{\beta(\lambda_1 h)^3}{6\alpha}+\frac{\beta(\lambda_1 h)^3}{2\alpha}+\frac{1-[1+4\alpha\beta(\lambda_1 h)]^{\frac{5}{2}}}{120\alpha^4\beta^2}\right.\right.$$
$$\left.-\frac{(\lambda_1 h)[1+4\alpha\beta(\lambda_1 h)]^{\frac{3}{2}}}{12\alpha^3\beta}\right]/h+\left[-\frac{h^2-(\lambda_2 h)^2}{4\alpha^2}-\frac{\beta(h^3-(\lambda_2 h)^3)}{6\alpha}\right.$$
$$+\frac{\beta h^3(\lambda_2-\lambda_2^3)}{2\alpha}+\frac{[1+4\alpha\beta(h-\lambda_2 h)]^{5/2}-1}{120\alpha^4\beta^2}+\frac{h^2(1-\lambda_2)}{2\alpha^2} \qquad (4.3)$$
$$\left.+\frac{\beta h^3\left(\lambda_2-{\lambda_2}^2\right)}{2\alpha}-\frac{(h-\lambda_2 h)[1+4\alpha\beta(h-\lambda_2 h)]^{\frac{3}{2}}}{12\alpha^3\beta}-v_p(h-\lambda_2 h)\right]/h$$
$$\left.+\left(\frac{\lambda_1 h}{2\alpha^2}+\frac{\beta(\lambda_1 h)^2}{2\alpha}+\frac{1}{12\alpha^3\beta}-\frac{[1+4\alpha\beta(\lambda_1 h)]^{3/2}}{12\alpha^3\beta}\right)(\lambda_2-\lambda_1)\right\}-\bar{v}=0$$

Flow diagram in Figure 4.1 shows the steps to derive equations of HBE model.

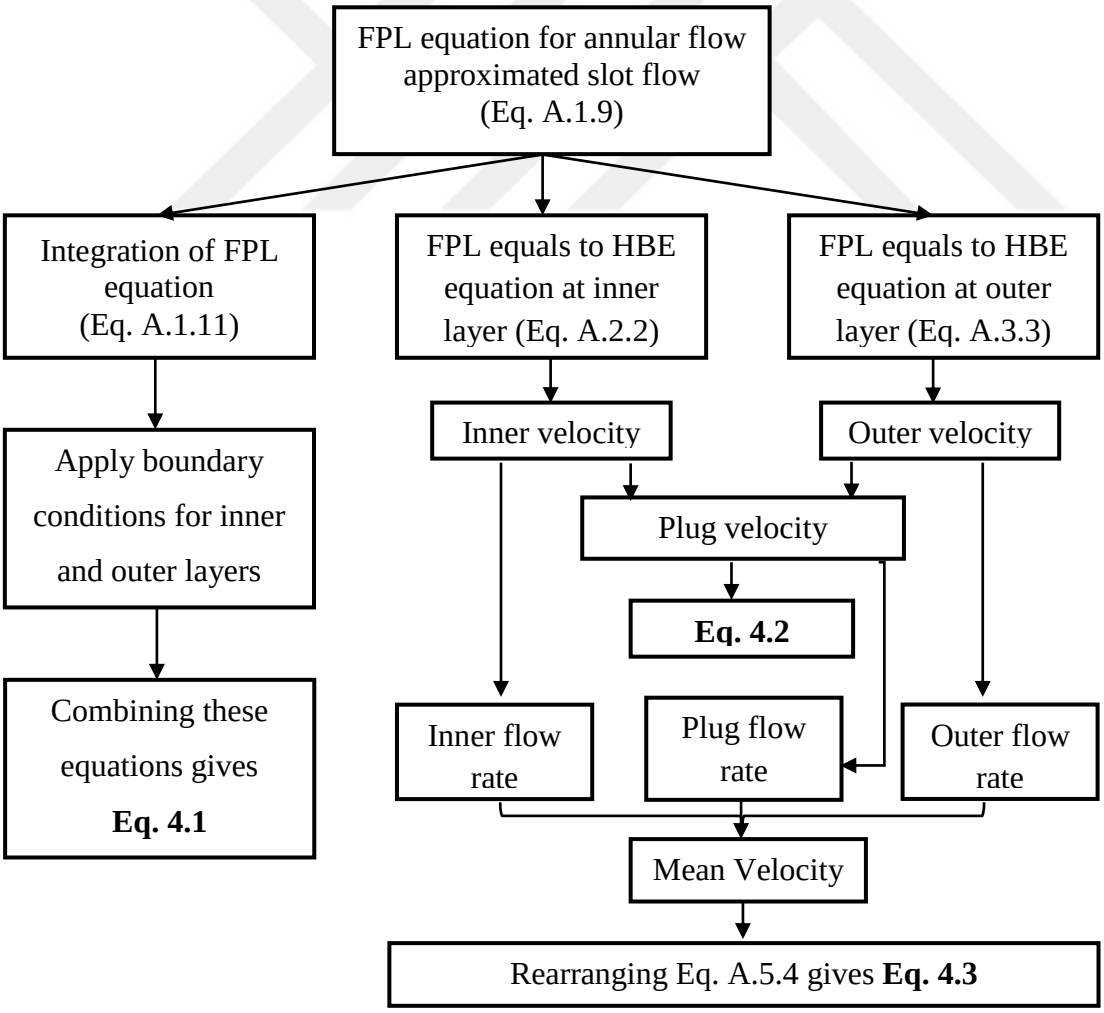

Figure 4.1: Flow chart of equations derived for HBE model.

5. APPLICATION TO SURGE-SWAB PRESSURES

Since there is not enough rheological parameters of Extended Herschel Bulkley fluid in the literature, they are generated by using the field mud data is taken by paper of Merlo et al, 1995 is presented in Table 5.1:

Table 5.1: Mud rheology measurements.

Rotor Speed (rpm)	Dial Reading (lb_F/100sqft)	Shear Rate (s^{-1})	Shear Stress (Pa)
600	52	1021.80	24.90
300	38	510.90	18.20
200	33	340.60	15.80
100	26	170.30	12.45
6	11	10.22	5.27
3	7	5.11	3.35

Rheological parameters according to Table 5.1 are calculated by Matlab code of Nguimatsia (2019) which is presented in Table 5.2 for Bingham plastic (BP), Herschel-Bulkley (HB) and Extended Herschel-Bulkley (HBE) fluid.

Table 5.2: Calculated rheological parameters (Nguimatsia, 2019).

	BP		HB		HBE	
	4-Readings	6-Readings	4-Readings	6-Readings	4-Readings	6-Readings
τ_0, Pa	6.8986	11.2577	7.538	1.702	6.4201	2.376
$K, Pa.s^n$	-	-	0.192	1.206	0.46	0.837
$\mu_p, Pa.s$	0.0213	0.0152	-	-	-	-
$\mu_\infty, Pa.s$	-	-	-	-	0.0053	-0.0027
n	-	-	0.663	0.435	0.5	0.5

Since Extended Herschel-Bulkley fluid are effective in high shear rate, the constant viscosity calculated using 6 readings has negative value. Therefore, rheological parameters according to these readings are calculated using 4 readings within shear rate range from 100 rpm to 600 rpm.

Hereinafter, frictional pressure gradient will be calculated using these parameters for each rheological model for uniform (open-ended pipe) and non-uniform geometry. The overall upward flow rate of drilling fluid due to running pipe into the borehole is required to be identical with amount but in reverse direction to the flow rate where fluid is removed from the bottom of the hole through the designated pipe region. Similarly, the overall downward flow rate of drilling fluid due to pulling pipe from the borehole is required to be identical with amount but in reverse direction to the volume rate where pipe is being withdrawn. If the bottom of the pipe is closed, the magnitude of the average velocity is given by,

$$\bar{v}_a = \frac{d_1^2 v_p}{(d_2^2 - d_1^2)} \tag{5.1}$$

If the pipe is open-ended, upright pipe motion will lead to flowing both in the pipe and in the annulus. However, since the pipe and annulus have a common pressure at both the top and the bottom, total frictional pressure loss must be same inside the pipe and the annulus. As the coupled flow in pipe and annulus must be identical with amount of the rate where pipe is run into or pull out of the wellbore, average annular velocity ($\bar{v}_a$) is indicated for laminar flow arising from the vertical motion of an open-ended pipe with uniform geometry with the following equation:

$$\bar{v}_a = v_p \frac{3d^4 - 4d_1^2(d_2 - d_1)^2}{-6d^4 - 4(d_2 - d_1)^2(d_2^2 - d_1^2)} \tag{5.2}$$

While using Equation 5.2, the direction of fluid movement is considered reverse with the direction of pipe motion in the derivation calculations. While pipe motion is ascending, the calculated frictional pressure difference at the bottom of the pipe is going to bring about the pressure decline. Likewise, while pipe motion is descending, the bottomhole frictional pressure difference is going to bring about the pressure increment.

5.1 Uniform Geometry Run Case

Example of a uniform geometry is used with the properties 10.75-in. (0.27305 m) casing (having a 10.0-in. (0.254m) ID) is being lowered at a rate of 1.0 ft/s (0.3048 m/s) in a 12-in (0.3048 m) hole.

If the bottom of the casing is open, the mean annular velocity is given by Equation 5.2:

$$\bar{v}_a = (1)\frac{3(10)^4 - 4(10.75)^2(12-10.75)^2}{-6(10)^4 - 4(12-10.75)^2(12^2-10.75^2)} = -0.4865\ ft/s$$

The viscous pressure gradient is given with field units for Bingham plastic fluid by Equation 1.9:

$$\frac{dp_f}{dL} = \frac{(21.3)(1-0.4865)}{1000\ (12-10.75)^2} + \frac{14.41}{200\ (12-10.75)} = 0.0646\ psi/ft$$

Frictional pressure gradient is found as 0.0646 psi/ft (1.462 kPa/m) for Bingham plastic fluid.

Similarly, Equations from 1.17 to 1.34 are used to calculate frictional pressure gradient for Herschel-Bulkley fluid in SI units. Firstly, the flow rate has been found as 0.0022 m^3/s. Then, Ca is calculated as 0.577. Finally, frictional pressure gradient is found as 1.527 kPa/m (0.0675 psi/ft).

For Extended Herschel-Bulkley fluid model, Equations A.1.16, A.4.6 and A.5.4 have been used to calculate the frictional pressure gradient. These three unknowns have been calculated as $\lambda_1 = 0.337$, $\lambda_2 = 0.87$ and frictional pressure gradient is 1.518 kPa/m (0.0671 psi/ft). The results are compared in Table 5.3.

Table 5.3: Comparing new method for uniform geometry (open-ended).

Model	$\boldsymbol{dp_f/dL}$	
	In field units, psi/ft	**In SI units, kPa/m**
BP	0.0646	1.462
HB	0.0675	1.527
HBE	0.0671	1.518

If the bottom of the casing is closed, the mean annular velocity is given by Equation 5.1:

$$\bar{v}_a = \frac{(10.75)^2\ (0.3048)}{(12^2 - 10.75^2)} = 4.064\ ft/s$$

The viscous pressure gradient is given with field units for Bingham plastic fluid by Equation 1.9:

$$\frac{dp_f}{dL} = \frac{(21.3)(1+4.064)}{1000\ (12-10.75)^2} + \frac{14.41}{200\ (12-10.75)} = 0.127\ psi/ft$$

Frictional pressure gradient is found as 0.127 psi/ft (2.865 kPa/m) for Bingham plastic fluid.

Similarly, Equations from 1.17 to 1.34 are used to calculate frictional pressure gradient for Herschel-Bulkley fluid in SI units. Firstly, the flow rate has been found as 0.002 m^3/s. Then, Ca is calculated as 0.785. Finally, frictional pressure gradient is found as 2.955 kPa/m (0.13 psi/ft).

For Extended Herschel-Bulkley fluid model, Equations A.1.16, A.4.6 and A.5.4 have been used to calculate the frictional pressure gradient. These three unknowns have been calculated as $\lambda_1 = 0.317$, $\lambda_2 = 0.596$ and frictional pressure gradient is 2.898 kPa/m (0.128 psi/ft). The results are compared in Table 5.4.

Table 5.4: Comparing new method for uniform geometry (closed-ended).

Model	dp_f/dL	
	In field units, psi/ft	**In SI units, kPa/m**
BP	0.127	2.865
HB	0.13	2.955
HBE	0.128	2.898

5.2 Non-Uniform Geometry Run Case

For uniform annular geometry, while running casing, the frictional pressure difference is uniform and easy as well. On the other hand, for a non-uniform pipe for instance a drillstring containing drillpipe, drill collars, and bit jets, a complex problem must be determined by employing an iterative method as in the case with our drillstring which is shown in Figure 5.1. And the properties of that drillstring are indicated below in Table 5.5.

Calculations:

For simplicity, the influence of tool intersections is considered to be non-effective and is ignored. Furthermore, it is considered that borehole is maintained full and that the fluid line in the pipe and annuli are retained approximately equivalent. Pipe and annular divisions are numerated beginning at the bottom of the drillstring and expressed below.

i=1 : bit jets; i=2 : drill collar , i=3 : drill pipe

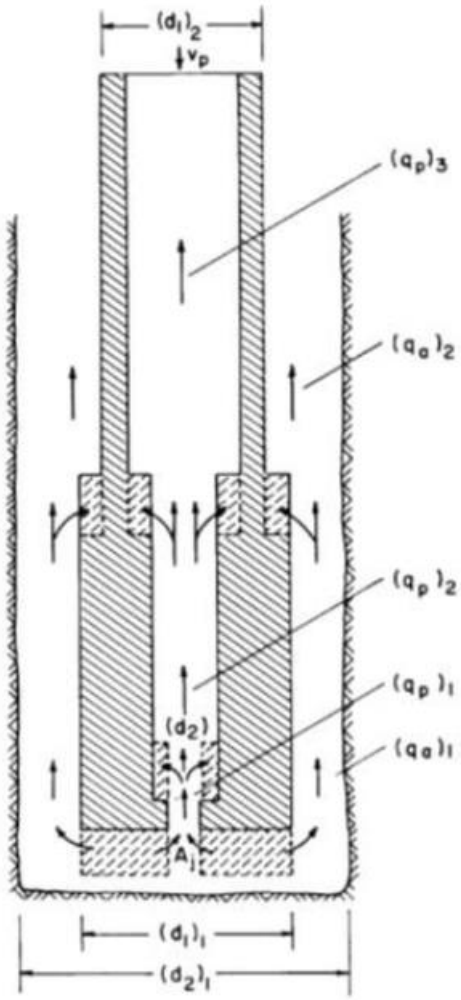

Figure 5.1: Hydraulic interpretation of a drillstring in non-uniform case (Bourgoyne et al., 1991).

The overall flow rate nearby the bottom of the drillstring is defined by:

$$q_t = v_p \left[\frac{\pi}{4}(d_1)^2 - A_j\right] \tag{5.3}$$

where $v_p = 4\, ft/s = 1.2192\, m/s$

$$q_t = 1.2192 \left[\frac{\pi}{4}(0.1587)^2 - 0.00018\right] = 0.02391 \quad [m^3/s]$$

The flow rate over the bit jets is defined by,

$$\left(q_p\right)_1 = (1 - f_a)(q_t)_1 \tag{5.4}$$

where f_a is the ratio of the annulus flow rate to total flow rate.

$$\left(q_p\right)_1 = (1 - f_a)(0.02391) \quad [m^3/s]$$

Table 5.5: Well configurations.

Component	Parameter	Imperial Units	SI Units
Drillstring	Hole diameter	7.875 in	0.20003 m
	Length	15000 ft	4572 m
Drillpipe	OD	4.5 in	0.1143 m
	ID	3.826 in	0.09718 m
	Length	14300 ft	4358.64 m
Drill collar	OD	6.25 in	0.1587 m
	ID	2.75 in	0.06985 m
	Length	700 ft	213.36 m
Bit	Three nozzles	11/32 in	0.008731 m
	Discharge area	0.2784 in^2	0.00018 m^2
	Discharge coef.	0.95	0.95

The flow rates in drill collar and drill pipe interior are defined by

$$\left(q_p\right)_i = \left(q_p\right)_{i-1} - \frac{\pi}{4} v_p [(d)_i^2 - (d)_{i-1}^2] \tag{5.5}$$

For drill collar (i=2):

$$\left(q_p\right)_2 = (1 - f_a)(0.02391) - (1.2192)\left[\frac{\pi}{4}(0.06985)^2 - 0.00018\right]$$

$$\left(q_p\right)_2 = (0.02391)(1 - f_a) - 0.004452 \quad [m^3/s]$$

For drill pipe (i=3):

$$\left(q_p\right)_3 = (0.02391)(1 - f_a) - 0.004452 - (1.2192)\frac{\pi}{4}[(0.09718)^2 - (0.06985)^2]$$

$$\left(q_p\right)_3 = (0.02391)(1 - f_a) - 0.008823 \quad [m^3/s]$$

The mean velocity (regarding a viewer at the surface) equals to

$$(v_e)_i = \left(q_p\right)_i / \left(A_p\right)_i \tag{5.6}$$

For Bit jets (i=1):

$$(v_e)_1 = \frac{(0.02391)(1 - f_a)}{0.00018} = 132.83(1 - f_a) \quad [m/s]$$

For drill collar (i=2):

$$(v_e)_2 = \frac{(0.02391)(1 - f_a) - 0.004452}{\frac{\pi}{4}\,(0.06985)^2}$$

$$(v_e)_2 = (6.24)(1 - f_a) - 1.1618 \quad [m/s]$$

For drill pipe (i=3):

$$(v_e)_3 = \frac{(0.02391)(1 - f_a) - 0.008823}{\frac{\pi}{4}\,(0.09718)^2}$$

$$(v_e)_3 = (3.22)(1 - f_a) - 1.1895 \quad [m/s]$$

The effective fluid velocity (as regards the nozzle wall) through the bit jets is defined by,

$$(v_{ie})_i = (v_e)_i + v_p \tag{5.7}$$

Then

$$(v_{ie})_1 = (132.83)(1 - f_a) + 1.2192 \quad [m/s]$$

$$(v_{ie})_2 = (6.24)(1 - f_a) + 0.0574 \quad [m/s]$$

$$(v_{ie})_3 = (3.22)(1 - f_a) + 0.0297 \quad [m/s]$$

The pressure drop throughout the bit jets, Δp_b, is computed by readjustment of Equation 5.8 presented in Field units by replacing $(v_{ie})_1$ instead of v_n. The frictional pressure drops throughout the drill collars and drill pipe are computed employing the flow equations given in the first chapter and beginning of this chapter by substituting $(v_{ie})_2$ and $(v_{ie})_3$, respectively. The frictional pressure drops for each division are computed for both in laminar and in turbulent regime, and then the greater of the two outcomes is considered as the accurate value.

$$v_n = C_d \sqrt{\frac{\Delta p_b}{8.074x10^{-4}\rho}} \tag{5.8}$$

Frictional pressure drops in the annulus are calculated applying a procedure close to that applied to the pipe interior by determining effective annular velocities. The flow rates in Sections 1 and 2 of the drill collar and drill pipe annulus are defined below:

$$(q_a)_1 = f_a(q_t)_1 \tag{5.9}$$

$$(q_a)_1 = (0.02391\ f_a) \quad [m^3/s]$$

$$(q_a)_i = (q_a)_{i-1} - \frac{\pi}{4} v_p[(d_1)_{i-1}^2 - (d_1)_i^2] \tag{5.10}$$

$$(q_a)_2 = (q_a)_1 - \frac{\pi}{4} v_p[(d_1)_1^2 - (d_1)_2^2]$$

$$(q_a)_2 = (0.02391\ f_a) - \frac{\pi}{4}(1.2192)[(0.15875)^2 - (0.1143)^2]$$

$$(q_a)_2 = (0.02391\ f_a) - 0.01163 \quad [m^3/s]$$

The mean annular velocity (regarding a viewer at the surface) is defined by

$$(v_a)_1 = \frac{(q_a)_1}{(A_a)_1} \tag{5.11}$$

$$(v_a)_1 = \frac{(0.02391\ f_a)}{\frac{\pi}{4}(0.20003^2 - 0.15875^2)} = (2.0551\ f_a) \quad [m/s]$$

$$(v_a)_2 = \frac{(0.02391\ f_a) - 0.01163}{\frac{\pi}{4}(0.20003^2 - 0.1143^2)} = (1.1297\ f_a - 0.5495) \quad [m/s]$$

The effective annular velocity is expressed by $\bar{v}_a + K v_p$ where the mud clinging constant, K, is described by Figure 5.2. The ratio d_1/d_2 is found as 0.571 for the drill pipe and 0.794 for the drill collar. Fontenot and Clark (1974) developed equations to determine mud clinging constant as expressed with the following equations.

Drill pipe;

For laminar flow:

$$K = \frac{\alpha^2 - 2\alpha^2\ ln\alpha - 1}{2(1-\alpha^2)\ ln\alpha} \tag{5.12}$$

$$K = \frac{0.571^2 - 2(0.571)^2 \ln(0.571) - 1}{2(1-0.571^2)\ln(0.571)} = 0.409$$

For turbulent flow:

$$K = \frac{\sqrt{\frac{\alpha^4 + \alpha}{1+\alpha}} - \alpha^2}{1-\alpha^2} \tag{5.13}$$

$$K = \frac{\sqrt{\frac{0.571^4 + 0.571}{1 + 0.571}} - 0.571^2}{1 - 0.571^2} = 0.490$$

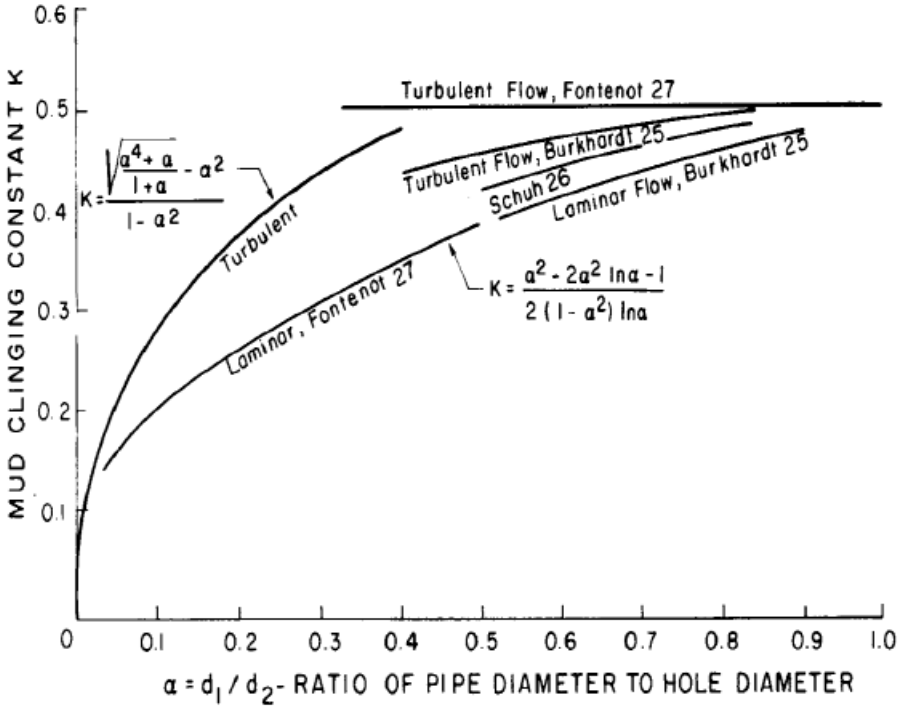

Figure 5.2: Determination of mud clinging constant (Bourgoyne et al., 1991).

Drill collar;

For laminar flow:

$$K = \frac{0.794^2 - 2(0.794)^2 \ln(0.794) - 1}{2(1 - 0.794^2)\ln(0.794)} = 0.462$$

For turbulent flow:

$$K = \frac{\sqrt{\frac{0.794^4 + 0.794}{1 + 0.794}} - 0.794^2}{1 - 0.794^2} = 0.499$$

Consequently, the effective annular velocity corresponding the drill collar is

$$(v_{ae})_i = (v_a)_i + Kv_p \tag{5.14}$$

$$(v_{ae})_1 = (2.0551\ f_a) + (0.462)(1.2192)$$
$$= (2.0551\ f_a) + 0.5633 \quad [m/s] \qquad for\ laminar\ flow$$

$$(v_{ae})_1 = (2.0551\ f_a) + (0.499)(1.2192)$$
$$= (2.0551\ f_a) + 0.6084 \quad [m/s] \quad for\ turbulent\ flow$$

In the same way, the effective annular velocity corresponding the drill pipe is

$$(v_{ae})_2 = (1.1297\ f_a - 0.5495) + (0.409)(1.2192)$$
$$= 1.1297\ f_a - 0.0508 \quad [m/s] \quad for\ laminar\ flow$$

$$(v_{ae})_2 = (1.1297\ f_a - 0.5495) + (0.490)(1.2192)$$
$$= 1.1297\ f_a + 0.0479 \quad [m/s] \quad for\ turbulent\ flow$$

Since there are two situations in annuli for each division in consideration of laminar and turbulent regime, so frictional pressure drops will be computed for each situation and the greater of the two outcomes is chosen as the accurate value.

For Bingham plastic fluid:

Note that since pressure loss equations for Bingham plastic fluid are expressed in field units in the first chapter, calculations are made in field units but results presented in Table 5.6 in SI units.

Table 5.6: Summary of surge pressure calculation for BP.

Variable		
f_a	0.5	0.7144
$(q_p)_1$ m^3/s	0.012	0.0068
$(q_p)_2$ m^3/s	0.0075	0.0024
$(q_p)_3$ m^3/s	0.0031	-0.002
Δp_b, kPa	3055	1044.9
Δp_{dc}, kPa	553.8	216.6
Δp_{dp}, kPa	2357	1951.4
Total Δp_i, kPa	5966.1	3212.9
$(q_a)_1$ m^3/s	0.012	0.0171
$(q_a)_2$ m^3/s	0.0003	0.0055
Δp_{dca}, kPa	431.7	651.8
Δp_{dpa}, kPa	2415.4	2559.9
Total Δp_a, kPa	2847.1	3211.8

Frictional pressure losses for Δp_{dc}, Δp_{dp}, and $\Delta p_{dca}$is greater in turbulent regime than in laminar regime. Therefore, pressure loss calculations for turbulent regime have been

used and presented in Table 5.6. On the other hand, Δp_{dpa} is greater in laminar regime than in turbulent regime.

For Herschel-Bulkley fluid:

Similar to Bingham plastic fluid, surge pressures are calculated for Herschel-Bulkley fluid as shown in Table 5.7. Same flow regions are valid also for Herschel-Bulkley fluid.

Table 5.7: Summary of surge pressure calculation for HB.

Variable		
f_a	0.5	0.7234
$(q_p)_1$ m^3/s	0.012	0.0066
$(q_p)_2$ m^3/s	0.0075	0.0022
$(q_p)_3$ m^3/s	0.0031	-0.0022
Δp_b, kPa	3055.3	962.4
Δp_{dc}, kPa	514.6	210.8
Δp_{dp}, kPa	2653.8	2177
Total Δp_i, kPa	6223.7	3350.2
$(q_a)_1$ m^3/s	0.012	0.0173
$(q_a)_2$ m^3/s	0.0003	0.0057
Δp_{dca}, kPa	461.3	510.2
Δp_{dpa}, kPa	2575	2838.5
Total Δp_a, kPa	3036.3	3348.7

For Extended Herschel-Bulkley fluid:

New semi-analytical method is valid for laminar flow. Therefore, frictional pressure loss calculations in turbulent regime will be made by using Herschel-Bulkley fluid. Since frictional pressure loss for only drill collar region is in turbulent regime, only that parameter will be calculated using Herschel-Bulkley as shown in Table 5.8.

New semi-analytical method predicting pressure surges for Extended-Herschel Bulkley fluid is compared of total pressure losses for these three model is tabulated in Table 5.9.

Table 5.8: Summary of surge pressure calculation for HBE.

Variable		
f_a	0.5	0.718
$(q_p)_1$ m^3/s	0.012	0.0067
$(q_p)_2$ m^3/s	0.0075	0.0023
$(q_p)_3$ m^3/s	0.0031	-0.0021
Δp_b, kPa	3055.3	999.1
Δp_{dc}, kPa	514.6	217
Δp_{dp}, kPa	2653.8	2229.5
Total Δp_i, kPa	6223.7	3445.6
$(q_a)_1$ m^3/s	0.012	0.0172
$(q_a)_2$ m^3/s	0.0003	0.0055
Δp_{dca}, kPa	392.6	441.7
Δp_{dpa}, kPa	2752.8	3007.5
Total Δp_a, kPa	3145.4	3449.1

Table 5.9: Summary of total surge pressure calculations.

Model	f_a	Total $\Delta p, kPa$	Total $\Delta p, psi$
BP	0.7144	3212.8	466
HB	0.7234	3348.7	485.6
HBE	0.718	3449.1	499.7

Hence the results indicate that the total pressure loss beneath the drillstring due to upward movement of pipe is 466 psi and 71.44% of the flow at the bottom of drill string is from the annulus and 28.56% of flow is from the interior of the drill string for Bingham plastic fluid.

Similarly, the total pressure loss beneath the drillstring due to upward movement of pipe is 485.6 psi and 72.34% of the flow at the bottom of drill string is from the annulus and 27.66% of flow is from the interior of the drill string for Herschel-Bulkley fluid.

Lastly, the total pressure loss beneath the drillstring due to upward movement of pipe is 499.7 psi and 71.8% of the flow at the bottom of drill string is from the annulus and 28.2% of flow is from the interior of the drill string for Extended Herschel-Bulkley fluid.

One of most important parameter in pressure surges is tripping speed, total frictional pressure loss (psi) and equivalent density (lbm/gal) at a depth of 15000 ft for this surge pressure is calculated for various pipe velocities (ft/s) and tabulated in table 5.10 in field units.

Table 5.10: Effect of pipe speed for non-uniform geometry case.

	Bingham Plastic			**Herschel-Bulkley**			**Extended-HB**		
$\mathbf{V_p}$	$\mathbf{f_a}$	Δp	ρ_e	$\mathbf{f_a}$	Δp	ρ_e	$\mathbf{f_a}$	Δp	ρ_e
1	0.27	346	10.46	0.45	328	10.43	0.38	331	10.44
2	0.56	378	10.5	0.6	390	10.51	0.572	405	10.53
3	0.672	409	10.54	0.675	441	10.58	0.668	465	10.61
4	0.712	465	10.61	0.7234	485	10.64	0.718	500	10.66
5	0.734	533	10.7	0.751	540	10.71	0.748	543	10.71
6	0.747	613	10.8	0.768	601	10.79	0.761	605	10.79
8	0.7445	930	11.21	0.788	746	10.97	0.771	761	10.99

The relationship between pressure surges and pipe velocities depends on a number of drilling parameters including fluid rheology and borehole geometry. The pressure surges are increasing with increasing tripping speed. It can also be seen that the annular fraction flow is rising, which means that the drilling fluid starts displacing more from the annulus rather than from pipe interior.

5.3 Results and Discussions

Pressure surges were calculated in the case of uniform (open-ended and closed-ended pipe) and non-uniform geometry for Bingham plastic, Herschel-Bulkley and Extended Herschel-Bulkley fluids. For open-ended pipe case, calculated frictional pressure gradient is consistent for Herschel-Bulkley and Extended Herschel-Bulkley fluids. Calculated frictional pressure gradient for Bingham plastic fluid has lower value in comparison with HB and HBE fluids.

In the case of closed-ended pipe, calculated frictional pressure gradient values are very close to each other for all implemented rheological fluids. This is because average pipe speed in closed-ended pipe case is much more than pipe speed in open-ended pipe case since there is no flow through the pipe interior and flow rate ratio (f_a) is known to be equal to one.

Calculating frictional pressure loss for non-uniform geometry requires iteration procedure to estimate flow rate ratio to make total pressure loss in equilibrium inside the pipe and annulus. Flow rate ratio values (f_a) are close to each other for all implemented rheological models. Total pressure loss value for HB fluid is between BP and HBE fluids. It can be said that developed pressure surge equations give good results.

Finally, Herschel-Bulkley model and Extended Herschel-Bulkley model give consistent results for various tripping speeds. The difference in flow rate ratio between rheological fluid models (especially Bingham plastic fluid) is increasing at very low pipe speeds. Flow rate ratio is becoming stable after certain pipe velocity. Also, for Bingham plastic fluid, flow ratio is stop increasing at pipe velocity equals to 6 ft/s and flow ratio has lower value at pipe velocity equals to 8 ft/s than at pipe velocity equals to 6 ft/s. Moreover, total frictional pressure loss at pipe velocity equals to 8 ft/s for Bingham plastic fluid is more than other rheological models at pipe velocity equals to 8 ft/s. Therefore, it can be said that Bingham plastic model is not appropriate to predict total frictional pressure loss at high tripping velocities.

6. CONCLUSIONS

New semi analytical surge pressure model for HBE fluid was developed first time ever in this study. In the light of the results, it has been seen that new semi analytical surge pressure model for HBE fluid shows good agreement with the most accepted non-Newtonian models. Since developed equations for HBE fluid can be solved with simple computer code, it is appropriate to use in the field.

Commonly used rheological models (HB, BP, PL) in drilling engineering applications are only able to determine apparent Newtonian viscosities in low shear rate ranges (5.11-1022 sec^{-1}). Model validation has to be carried out in the low range of shear rate values since HB, BP and PL models have constraints or limitations at high shear rates.

Since HBE model has four parameter to be determined, it has capability of calculating apparent Newtonian viscosities at extremely high shear rates. Beside, HBE is capable of determining apparent Newtonian viscosities in the all ranges of shear rates, including classical field viscometer ranges (Fann VGR).

Due to the mathematical representation, HBE can be solved only for flow behavior index value of 0.5, there exists semi analytical solution for the HBE model when n is equal to 0.5. If n has a value other then 0.5, numerical solution is available that is out of the scope of this thesis.

Semi analytical solution for HBE model with n=0.5 was developed in this study for the first time ever in the literature. Developed model equations were used to determine surge-swab pressures in a realistic borehole conditions that constitutes different drillstring sizes along with considering both open-ended and closed-ended string runs.

At low shear rate ranges, both HBE and HB resulted in very similar results that are the clear proof of validity for the HBE model developed in the study.

REFERENCES

Bing, Z., Kaiji, and Z., Qiji, Y. (1995). Equations help calculate surge and swab pressures in inclined well. *Oil Gas J.* 93, 74–77.

Bourgoyne, A.T., Chenevert, E.M., Millheim, K.K., and Young, F.S. (1991). *Applied Drilling Engineering.* (SPE), Richardson, Texas.

Burkhardt, J.A. (1961). Wellbore pressure surges produced by pipe movement. *Journal of Petroleum Technology*, 13 (6), SPE-1546-G-PA, June 1961.

Canon, G.E. (1934). Changes in Hydrostatic pressure due to withdrawing drillpipe from the hole. *API Drilling and Production Practices,* 42-47.

Cardwell, W.T. (1953). Pressure changes in drilling wells caused by pipe movement. *API Drilling and Production Practices,* 97–112.

Clark, E.H. (1955). Bottom-hole pressure surges while running pipes. *Petrol. Eng. Int.* 68–96.

Clark, E.H. (1956). A graphic view of pressure surges and lost circulation. *API Drilling & Production Practices,* 424–438.

Crespo, F. (2011). *Experimental study and modeling on surge and swab pressures for Yield-power-law drilling fluids.* (MSc thesis). Mewbourne School of Petroleum & Geological Engineering, University of Oklahoma.

Crespo, F., Ahmed, R., Enfis, M., Saasen, A., Amani, M. (2012). Surge-and-swab pressure predictions for Yield-power-law drilling fluids. *SPE Drilling & Completions.*

Erge, O., Akin, S., Gucuyener, I.H. (2018). Accurate modelling of surge and swab pressures of yield power law fluids in concentric annuli, *SPE/IADC-189304-MS. In: SPE/IADC Middle East Drilling Technology Conference and Exhibition.* UAE, Abu Dhabi. https://doi.org/10.2118/189304-MS.

Ettehadi, A. (2016). *Modelling wellbore hydraulics through thermal rheological sepiolite mud properties.* (Dissertation). Istanbul Technical University, Graduate School of Science, Engineering and Technology.

Ettehadi, A., and Altun, G. (2018). Functional and practical analytical pressure surges model through Herschel Bulkley fluids, *Journal of Petroleum Science and Engineering.* 171 (2018) 748–759.

Fontenot, J.E. and Clark, R.K. (1974). An improved method for calculating swab and surge pressures and circulating pressures in a drilling well. *Soc. Petrol. Eng. J.* 451–462.

Goins, W.C., Weichhert, J.P., Burba, J.L., Dawson, D.D., Teplitz, A.J. (1951). Down-the-hole pressure surges and their effect on loss of circulation. *API Drilling and Production Practices*, 125–132.

Horn, A.J. (1950). Well blowouts in California drilling operations, causes and suggestions for prevention. *API Drilling and Production Practices*, 112–128.

Hussain, Q.E., and Sharif, M.A.R. (2009). Viscoplastic fluid flow in irregular eccentric annuli due to axial motion of the inner pipe. *Can. J. Chem. Eng.* 75 (6), 1038–1045.

Nguimatsia, J.D. (2019) *Determining parameters of rheological models by the method of least squares.* (MSc thesis). Istanbul Technical University, Graduate School of Science, Engineering and Technology.

Lal, M. (1983). Surge and swab modeling for dynamic pressures and safe trip velocities. *IADC/SPE Drilling Conference*, New Orleans, Louisiana, 20–23.

Lubinski, A., Hsu, F.H., Nolte, K.G. (1977). Transient pressure surges due to pipe movement in an oil well. *Oil & Gas Science and Technology*—Rev. IFP 32 (3), 307–348. https://doi.org/10.2516/ogst:1977019.

Madlener, K., Frey, B. and Ciezki, H. K. (2009). Generalized Reynolds number for non-Newtonian fluids. *Progr. Propul. Phys.* 1, 237–250.

Melrose, J. C., Savins, J. G., Foster, W. R., & Parish, E. R. (1958). A Practical Utilization of the Theory of Bingham Plastic Flow in Stationary Pipes and Annuli. *Society of Petroleum Engineers.* 316-324

Merlo.A, Maglione.R and Piatti.C. (1995). An innovative model for drilling fluid hydraulics. *SPE Asia Pascific Oil & Gas conference*, Kuala Lumpur, Malaysia.

Metzner, A.B., and J.C. Reed. (1955). Flow of non-Newtonian fluids - correlation of the laminar, transition and turbulent-flow regions. *AIChE J*. 1(4), 434-40.

Mitchell R.F. (1988). Dynamic surge and swab pressure predictions. *SPE Drilling Engineering.* 325–333. https://doi.org/10.2118/16156-PA.

Mooney, M. (1931). Explicit formulas for slip and fluidity. *J. Rheol.* 2(2), 210-22.

Ormsby, G.S. (1954). Calculation and control of mud pressures in drilling and completion operations. *API Drilling and Production Practices*, 44–55.

Rabinowitsch, B. (1929). Über die Viskositat und Elastizitat von Solen. *Z. Phys. Chem.* 145A.

Schuh, F.J. (1964). Computer makes surge-pressure calculations useful. *Oil Gas J*. 62 (31), 96–104.

Skalle, P. (2012). *Drilling Fluid Engineering*. Ventus publishing Aps.

Wang, Y., and Chukwu, G.A. (1997). Application of unsteady Couette flow of non-Newtonian power-law fluids in concentric annular wellbore. *J. Petrol. Sci. Eng.* 17, 229.

Yang, L. and Chukwu, G. A. (1995), A simplified couette flow solution of non-newtonian power-law fluids in eccentric annuli. *Can. J. Chem. Eng.*, 73: 241-247. doi:10.1002/cjce.5450730211

APPENDICES

APPENDIX A: Model derivation for HBE fluid

APPENDIX B: The Pyhton code

APPENDIX A

A.1 Narrow Slot Flow Approximation

The general solution of frictional pressure gradient for a non-Newtonian fluid can be employed to compute surge and swab pressure caused by the plate motion representing the annulus as a slot which is illustrated in Figure A.1. As reported by Bourgoyne et.al (1991), annular flow also can be approached with equations given for flow through rectangular slots. The slot flow equations are easier to deal and are fairly correct in consideration of the ratio d_1/d_2 is greater than 0.3. The minimum ratio is mostly exceeded in nearly all rotary drilling applications. As illustrated in Figure A.2, an annular zone can be displayed as a narrow slot having an area (A) and height (h), defined by:

$$A = Wh = \pi(r_2^2 - r_1^2) \tag{A.1.1}$$

where,

$$h = r_2 - r_1 \tag{A.1.2}$$

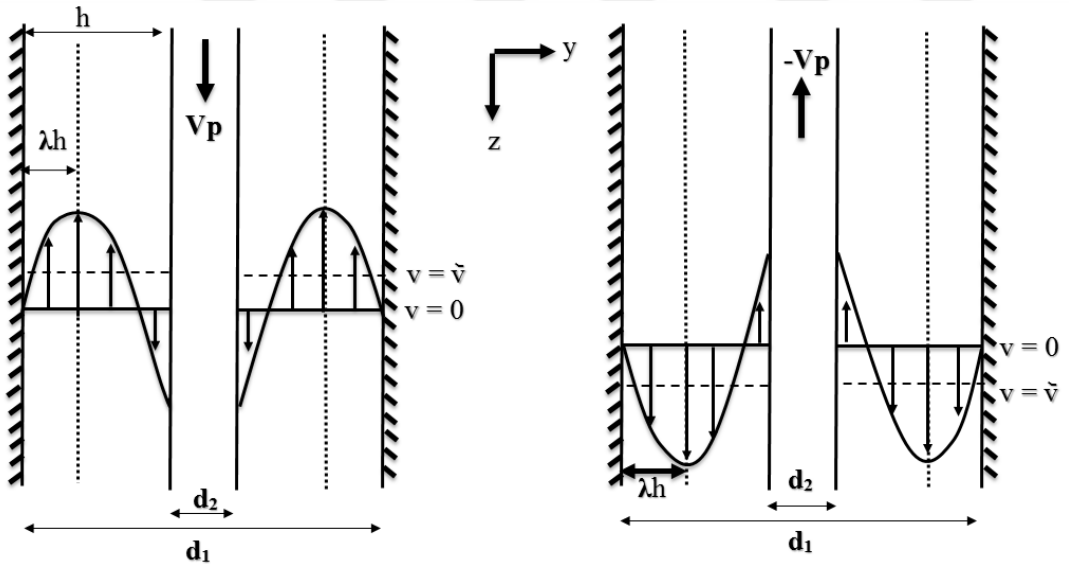

Figure A.1: Velocity profile for laminar flow caused by pipe movement, surge on the left – swab on the right (Ettehadi and Altun, 2018).

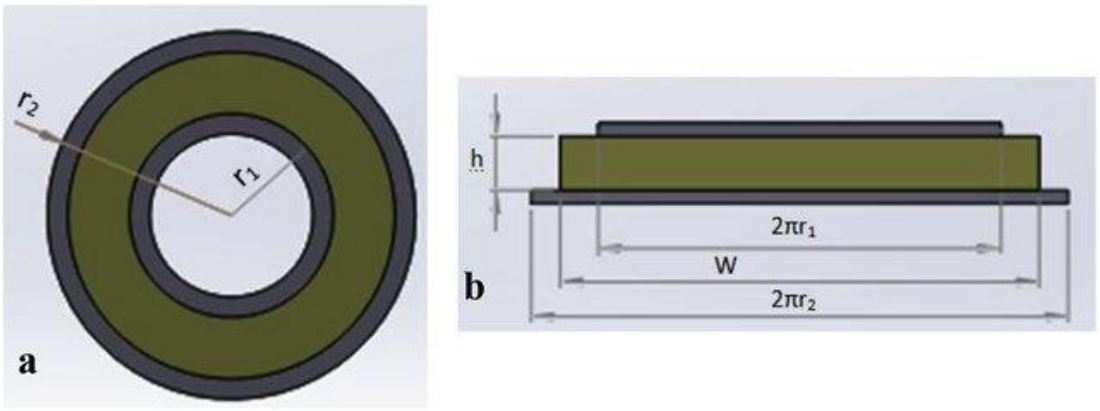

Figure A.2: Demonstrating the annuli in slot geometry: (a) circular and (b) rectangular (Bourgoyne et. al. 1991).

The relationship between shear stress and frictional pressure gradient for a slot can be acquired from a reply to the pressure and viscous drag forces conducting on a fluid element in the slot as illustrated in Figure A.3. If an element of fluid is considered having width (W) and thickness (Δy), the force (F_1) applied by the fluid pressure at first point is given by:

$$F_1 = p\ W\ \Delta y \tag{A.1.3}$$

Likewise, the force (F_2) applied by the fluid pressure at Point 2 is given by:

$$F_2 = p_2\ W\ \Delta y = \left(p - \frac{dp_f}{dL}\Delta L\right) W \Delta y \tag{A.1.4}$$

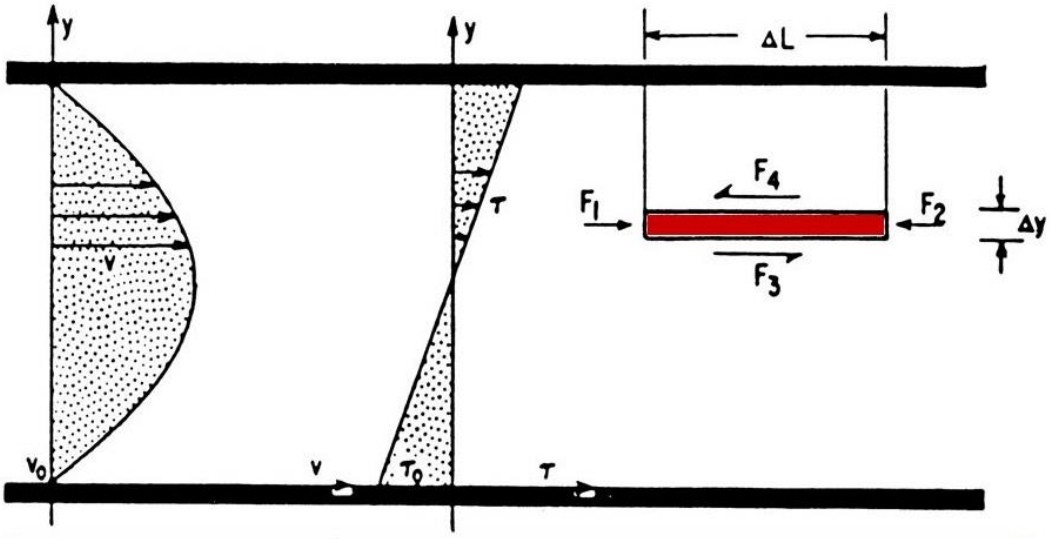

Figure A.3: Free body diagram for a fluid element in a narrow slot (Bourgoyne et al, 1991).

The frictional force exerted by the adjacent layer of fluid below the fluid element of interest is given by:

$$F_3 = \tau\, W\, \Delta L \tag{A.1.5}$$

Similarly, the frictional force exerted by the adjacent layer of fluid above the fluid element of interest is given by:

$$F_4 = \tau_{y+\Delta y}\, W\, \Delta L = \left(\tau + \frac{d\tau}{dy}\Delta y\right) W \Delta L \tag{A.1.6}$$

If the flow is steady, the sum of the forces acting on the fluid element must be equal to zero. Summing forces, we obtain:

$$F_1 - F_2 + F_3 - F_4 = 0 \tag{A.1.7}$$

And

$$p\, W\, \Delta y - \left(p - \frac{dp_f}{dL}\Delta L\right) W \Delta y + \tau\, W\, \Delta L - \left(\tau + \frac{d\tau}{dy}\Delta y\right) W \Delta L = 0 \tag{A.1.8}$$

Expanding this equation and dividing through by (WΔLΔy) yields:

$$\frac{dp_f}{dL} - \frac{d\tau}{dy} = 0 \tag{A.1.9}$$

This study depends on Equation A.1.9 that was used as an origin of the analytical solution for surge and swab pressures. Equation A.1.9 is applicable to be used for all rheological fluid models. Velocity profile of Extended Herschel-Bulkley fluid is identical to the Herschel-Bulkley fluid as illustrated in Figure A.4.

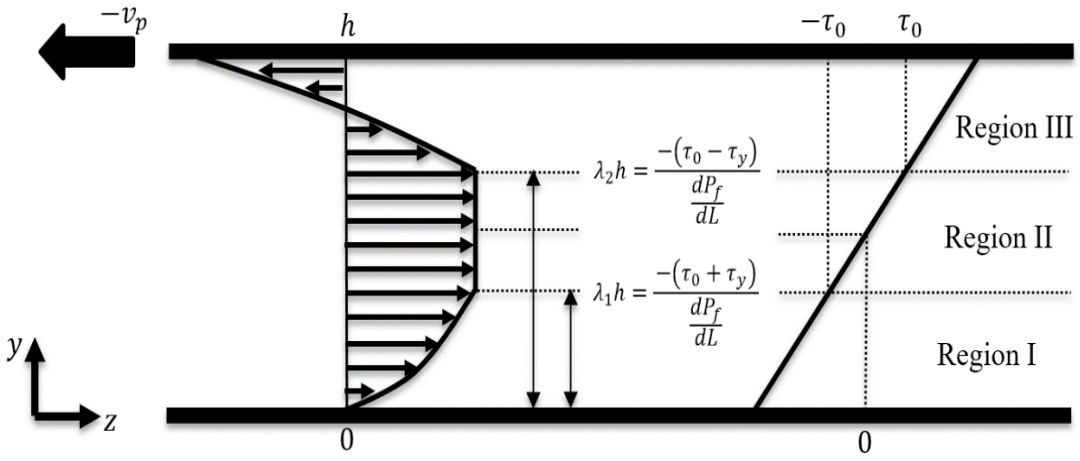

Figure A.4: Laminar flow of an Extended Herschel-Bulkley fluid in a slot (Ettehadi and Altun, 2018).

Equation A.1.9 can be integrated corresponding to thickness (y) as dp_f/dL is not a function of y because flow is only in horizontal direction. Separating variables and integrating gives:

$$\tau = y\frac{dP_f}{dL} + \tau_0 \tag{A.1.11}$$

where τ_0 represents the constant of integration that corresponds to the shear stress at y=0. In Figure A.4, slot geometry is separated three regions to solve equations according to these boundary conditions.

At the boundary, $y=\lambda_1 h$:

$$\tau_1 = -\tau_y = \tau_0 + \lambda_1 h\frac{dP_f}{dL} \qquad \rightarrow \qquad \tau_y + \tau_0 = -\lambda_1 h\frac{dP_f}{dL} \tag{A.1.12}$$

At the boundary, $y=\lambda_2 h$:

$$\tau_2 = \tau_y = \tau_0 + \lambda_2 h\frac{dP_f}{dL} \qquad \rightarrow \qquad \tau_y - \tau_0 = -\lambda_2 h\frac{dP_f}{dL} \tag{A.1.13}$$

If Equations A.1.12 and A.1.13 are rearranged and combined:

$$\lambda_2 h - \lambda_1 h = \frac{-(\tau_0 - \tau_y)}{\frac{dP_f}{dL}} + \frac{(\tau_0 + \tau_y)}{\frac{dP_f}{dL}} \tag{A.1.14}$$

$$h(\lambda_2 - \lambda_1) = \frac{2\tau_y}{\frac{dP_f}{dL}} \tag{A.1.15}$$

$$\frac{dP_f}{dL} - \frac{2\tau_y}{h(\lambda_2 - \lambda_1)} = 0 \tag{A.1.16}$$

Equation A.1.16 is the first equation which is used in iterative procedure. Hereafter, all regions are individually solved depending on boundary conditions.

A.2 Solution for Inner Layer (Region I)

For the sign convention used, shear stress (τ) has negative value while shear rate (γ) is positive regarding to Figure A.4. As a result, Equation 1.35 which is signified for Extended Herschel-Buckley fluids can be edited with respect to these situations.

$$\tau = -K\,(\gamma)^n - \mu_\infty(\gamma) - \tau_y \tag{A.2.1}$$

By using expression of shear stress defined in Equation A.1.11 and definition of shear rate, Equation A.2.1 can be written for inner layer as:

$$\tau_0 + y\frac{dP_f}{dL} = -K\left(\frac{dv}{dy}\right)^n - \mu_\infty\left(\frac{dv}{dy}\right) - \tau_y \tag{A.2.2}$$

where

$$\frac{dv}{dy} > 0 \quad \rightarrow \quad \gamma = -\frac{dv}{dy} < 0 \tag{A.2.3}$$

Equation A.2.2 can be rewritten as:

$$K\left(\frac{dv}{dy}\right)^n + \mu_\infty\left(\frac{dv}{dy}\right) = -(\tau_0 + \tau_y) - y\frac{dP_f}{dL} \tag{A.2.4}$$

By using the relation in Equation A.1.12, this equation becomes:

$$K\left(\frac{dv}{dy}\right)^n + \mu_\infty\left(\frac{dv}{dy}\right) = \lambda_1 h\frac{dP_f}{dL} - y\frac{dP_f}{dL} \tag{A.2.5}$$

Dividing Equation A.2.5 with K yields:

$$\left(\frac{dv}{dy}\right)^n + \frac{\mu_\infty}{K}\left(\frac{dv}{dy}\right) = \frac{1}{K}\frac{dP_f}{dL}[\lambda_1 h - \mathrm{y}] \tag{A.2.6}$$

Equation A.2.6 is first order nonlinear non-homogeneous ordinary differential equation. To solve this non-linear equation, n is assumed as n=0.5 and μ_∞/K is referred as "α" and $(dP_f/dL)/K$ is referred as "β" to make equation look simpler. Then,

$$\alpha\left(\frac{dv}{dy}\right) + \sqrt{\left(\frac{dv}{dy}\right)} = \beta\,[\lambda_1 h - \mathrm{y}] \tag{A.2.7}$$

Equation A.2.7 is made suitable in order to find its roots by dividing α and getting right side of the equation to left side as below:

$$\left(\frac{dv}{dy}\right) + \frac{1}{\alpha}\sqrt{\left(\frac{dv}{dy}\right)} - \frac{\beta}{\alpha}\,[\lambda_1 h - \mathrm{y}] = 0 \tag{A.2.8}$$

Now, changing variable for $\sqrt{dv/dy}$ = U gives:

$$U^2 + \frac{1}{\alpha}U - \frac{\beta}{\alpha}\left[\lambda_1 h - \mathrm{y}\right] = 0 \tag{A.2.9}$$

Roots of this equation can be found easily by finding discriminant.

$$U_1 = -\frac{1}{2\alpha} + \frac{1}{2\alpha}\sqrt{1 + 4\alpha\beta(\lambda_1 h - \mathrm{y})} \tag{A.2.10}$$

$$U_2 = -\frac{1}{2\alpha} - \frac{1}{2\alpha}\sqrt{1 + 4\alpha\beta(\lambda_1 h - \mathrm{y})} \tag{A.2.11}$$

To decide which root is going to be used, condition of the shear rate is considered. As shear rate (dv/dy) is positive in the inner layer, variable U which refers to $\sqrt{(dv/dy)}$ must be positive too. We know y is between 0 and $\lambda_1 h$.Therefore, $4\alpha\beta(\lambda_1 h - \mathrm{y})$ must be greater than or equal to 0. Then, $\sqrt{1 + 4\alpha\beta(\lambda_1 h - \mathrm{y})}$ must be greater than or equal to 1. Then, it yields:

$$U_1 = -\frac{1}{2\alpha} + \frac{1}{2\alpha}\sqrt{1 + 4\alpha\beta(\lambda_1 h - \mathrm{y})} \geq 0 \tag{A.2.12}$$

$$U_2 = -\frac{1}{2\alpha} - \frac{1}{2\alpha}\sqrt{1 + 4\alpha\beta(\lambda_1 h - \mathrm{y})} < 0 \tag{A.2.13}$$

As $(dv/dy) = U^2$, using this relationship for the first root gives

$$\frac{dv}{dy} = \left(-\frac{1}{2\alpha} + \frac{1}{2\alpha}\sqrt{1 + 4\alpha\beta(\lambda_1 h - \mathrm{y})}\right)^2 \tag{A.2.14}$$

Solution of the Equation A.2.14, gives:

$$\frac{dv}{dy} = \frac{1}{2}\left(\frac{1}{\alpha^2} - \frac{2\beta y}{\alpha} + \frac{2\beta(\lambda_1 h)}{\alpha} - \frac{\sqrt{1 + 4\alpha\beta(\lambda_1 h - \mathrm{y})}}{\alpha^2}\right) \tag{A.2.15}$$

Now, Equation A.2.15 can be integrated as below:

$$dv = \frac{1}{2}\left(\frac{1}{\alpha^2} - \frac{2\beta y}{\alpha} + \frac{2\beta(\lambda_1 h)}{\alpha} - \frac{\sqrt{1 + 4\alpha\beta(\lambda_1 h - \mathrm{y})}}{\alpha^2}\right)dy \tag{A.2.16}$$

$$v = \frac{y}{2\alpha^2} - \frac{\beta y^2}{2\alpha} + \frac{\beta(\lambda_1 h)y}{\alpha} + \frac{[1 + 4\alpha\beta(\lambda_1 h - \mathrm{y})]^{3/2}}{12\alpha^3\beta} + v_0 \tag{A.2.17}$$

The constant of integration, v_0, can be evaluated by employing the boundary condition that v=0 at y=0. Then,

$$0 = \frac{[1 + 4\alpha\beta(\lambda_1 h)]^{3/2}}{12\alpha^3\beta} + v_0 \tag{A.2.18}$$

$$v_0 = -\frac{[1 + 4\alpha\beta(\lambda_1 h)]^{3/2}}{12\alpha^3\beta} \tag{A.2.19}$$

Substituting the constant in Equation A.2.17 yields,

$$v_{inner} = \frac{y}{2\alpha^2} - \frac{\beta y^2}{2\alpha} + \frac{\beta(\lambda_1 h)y}{\alpha} + \frac{[1 + 4\alpha\beta(\lambda_1 h - \mathrm{y})]^{3/2}}{12\alpha^3\beta} - \frac{[1 + 4\alpha\beta(\lambda_1 h)]^{3/2}}{12\alpha^3\beta} \tag{A.2.20}$$

The flow rate in the $0 \leq \mathrm{y} \leq \lambda_1 h$ region can be found by taking integral of equation above where:

$$q = VdA = VWdy \tag{A.2.21}$$

Then, the flow rate is defined as:

$$q_{inner} = w \int_0^{\lambda_1 h} \left[\frac{y}{2\alpha^2} - \frac{\beta y^2}{2\alpha} + \frac{\beta(\lambda_1 h)y}{\alpha} + \frac{[1 + 4\alpha\beta(\lambda_1 h - \mathrm{y})]^{3/2}}{12\alpha^3\beta} - \frac{[1 + 4\alpha\beta(\lambda_1 h)]^{3/2}}{12\alpha^3\beta} \right] \tag{A.2.22}$$

$$q_{inner} = w \left[\frac{(\lambda_1 h)^2}{4\alpha^2} - \frac{\beta(\lambda_1 h)^3}{6\alpha} + \frac{\beta(\lambda_1 h)^3}{2\alpha} + \frac{1 - [1 + 4\alpha\beta(\lambda_1 h)]^{5/2}}{120\alpha^4\beta^2} - \frac{(\lambda_1 h)[1 + 4\alpha\beta(\lambda_1 h)]^{3/2}}{12\alpha^3\beta} \right] \tag{A.2.23}$$

A.3 Solution for Outer Layer (Region III)

Same approach in the first region can be applied to outer region with adding pipe velocity term and changing sign convention according to conditions. This region is existed for $\lambda_2 h \leq y \leq h$ and according to Figure A.4, sign is:

$$\frac{dv}{dy} < 0 \quad \rightarrow \quad \gamma = -\frac{dv}{dy} > 0 \tag{A.3.1}$$

As a result, Equation 1.35 which is signified for Extended Herschel-Buckley fluids can be edited with respect to these situations.

$$\tau = K\,(\gamma)^n + \mu_\infty(\gamma) + \tau_y \tag{A.3.2}$$

By using expression of shear stress (Equation A.1.11) and definition of shear rate for that interval, Equation A.3.2 can be written for outer layer as:

$$\tau_0 + y\frac{dP_f}{dL} = K\left(-\frac{dv}{dy}\right)^n + \mu_\infty\left(-\frac{dv}{dy}\right) + \tau_y \tag{A.3.3}$$

Equation A.3.3 can be rewritten as:

$$K\left(-\frac{dv}{dy}\right)^n + \mu_\infty\left(-\frac{dv}{dy}\right) = (\tau_0 - \tau_y) + y\frac{dP_f}{dL} \tag{A.3.4}$$

By using the relation in Equation A.1.13, this equation becomes:

$$K\left(-\frac{dv}{dy}\right)^n + \mu_\infty\left(-\frac{dv}{dy}\right) = y\frac{dP_f}{dL} - \lambda_2 h\frac{dP_f}{dL} \tag{A.3.5}$$

Dividing both side of the Equation A.3.5 with K yields:

$$\left(-\frac{dv}{dy}\right)^n + \frac{\mu_\infty}{K}\left(-\frac{dv}{dy}\right) = \frac{1}{K}\frac{dP_f}{dL}[y - \lambda_2 h] \tag{A.3.6}$$

To solve this non-linear equation, n is assumed as n=0.5 and μ_∞/K is referred as "α" and $(dP_f/dL)/K$ is referred as "β" to make equation look simpler. Then,

$$\alpha\left(-\frac{dv}{dy}\right) + \sqrt{\left(-\frac{dv}{dy}\right)} = \beta\,[y - \lambda_2 h] \tag{A.3.7}$$

Equation A.3.7 is made suitable by dividing α and getting right side of the equation to left side in order to find its roots as below:

$$\left(-\frac{dv}{dy}\right) + \frac{1}{\alpha}\sqrt{\left(-\frac{dv}{dy}\right)} - \frac{\beta}{\alpha}\,[y - \lambda_2 h] = 0 \tag{A.3.8}$$

Now, changing variable for $\sqrt{(-dv/dy)}$ = U gives:

$$U^2 + \frac{1}{\alpha}U - \frac{\beta}{\alpha}\,[y - \lambda_2 h] = 0 \tag{A.3.9}$$

Roots of this equation can be found easily by finding discriminant.

$$U_1 = -\frac{1}{2\alpha} + \frac{1}{2\alpha}\sqrt{1 + 4\alpha\beta(y - \lambda_2 h)} \tag{A.3.10}$$

$$U_2 = -\frac{1}{2\alpha} - \frac{1}{2\alpha}\sqrt{1 + 4\alpha\beta(y - \lambda_2 h)} \tag{A.3.11}$$

To decide which root is going to be used, condition of the shear rate is considered. As shear rate $(-dv/dy)$ is positive in the outer layer, variable U which refers to $\sqrt{(-dv/dy)}$ must be positive too. We know y is between $\lambda_2 h$ and h. Therefore, $4\alpha\beta(y - \lambda_2 h)$ must be greater than or equal to 0. Then, $\sqrt{1 + 4\alpha\beta(y - \lambda_2 h)}$ must be greater than or equal to 1. Then, it yields:

$$U_1 = -\frac{1}{2\alpha} + \frac{1}{2\alpha}\sqrt{1 + 4\alpha\beta(y - \lambda_2 h)} \geq 0 \tag{A.3.12}$$

$$U_2 = -\frac{1}{2\alpha} - \frac{1}{2\alpha}\sqrt{1 + 4\alpha\beta(y - \lambda_2 h)} < 0 \tag{A.3.13}$$

As $(-dv/dy) = U^2$, using this relationship for the first root gives

$$\left(-\frac{dv}{dy}\right) = \left(-\frac{1}{2\alpha} + \frac{1}{2\alpha}\sqrt{1 + 4\alpha\beta(y - \lambda_2 h)}\right)^2 \tag{A.3.14}$$

Solution of the Equation A.3.14, gives:

$$\left(-\frac{dv}{dy}\right) = \frac{1}{2}\left(\frac{1}{\alpha^2} + \frac{2\beta y}{\alpha} - \frac{2\beta(\lambda_2 h)}{\alpha} - \frac{\sqrt{1 + 4\alpha\beta(y - \lambda_2 h)}}{\alpha^2}\right) \tag{A.3.15}$$

$$\left(\frac{dv}{dy}\right) = -\frac{1}{2}\left(\frac{1}{\alpha^2} + \frac{2\beta y}{\alpha} - \frac{2\beta(\lambda_2 h)}{\alpha} - \frac{\sqrt{1 + 4\alpha\beta(y - \lambda_2 h)}}{\alpha^2}\right) \tag{A.3.16}$$

Now, Equation A.3.16 can be integrated as below:

$$dv = -\frac{1}{2}\left(\frac{1}{\alpha^2} + \frac{2\beta y}{\alpha} - \frac{2\beta(\lambda_2 h)}{\alpha} - \frac{\sqrt{1 + 4\alpha\beta(y - \lambda_2 h)}}{\alpha^2}\right) dy \tag{A.3.17}$$

$$v = -\frac{y}{2\alpha^2} - \frac{\beta y^2}{2\alpha} + \frac{\beta(\lambda_2 h)y}{\alpha} + \frac{[1 + 4\alpha\beta(y - \lambda_2 h)]^{3/2}}{12\alpha^3\beta} + v_c \tag{A.3.18}$$

The constant of integration, v_c, can be evaluated by employing the boundary condition that $v = -v_p$ at $y = h$. Then,

$$-v_p = -\frac{h}{2\alpha^2} - \frac{\beta h^2}{2\alpha} + \frac{\beta(\lambda_2 h^2)}{\alpha} + \frac{[1+4\alpha\beta(h-\lambda_2 h)]^{3/2}}{12\alpha^3\beta} + v_c \quad \text{(A.3.19)}$$

$$v_c = \frac{h}{2\alpha^2} + \frac{\beta h^2}{2\alpha} - \frac{\beta(\lambda_2 h^2)}{\alpha} - \frac{[1+4\alpha\beta(h-\lambda_2 h)]^{\frac{3}{2}}}{12\alpha^3\beta} - v_p \quad \text{(A.3.20)}$$

Substituting this constant in Equation A.3.8 yields,

$$\begin{aligned} v_{outer} = &-\frac{y}{2\alpha^2} - \frac{\beta y^2}{2\alpha} + \frac{\beta(\lambda_2 h)y}{\alpha} + \frac{[1+4\alpha\beta(y-\lambda_2 h)]^{3/2}}{12\alpha^3\beta} \\ &+ \frac{h}{2\alpha^2} + \frac{\beta h^2}{2\alpha} - \frac{\beta(\lambda_2 h^2)}{\alpha} - \frac{[1+4\alpha\beta(h-\lambda_2 h)]^{\frac{3}{2}}}{12\alpha^3\beta} - v_p \end{aligned} \quad \text{(A.3.21)}$$

The flow rate in the $\lambda_2 h \le y \le h$ region can be found by taking integral of equation above and using Equation A.2.21. So, the flow rate is defined as:

$$\begin{aligned} q_{outer} = w \int_{\lambda_2 h}^{h} \Bigg[&-\frac{y}{2\alpha^2} - \frac{\beta y^2}{2\alpha} + \frac{\beta(\lambda_2 h)y}{\alpha} + \frac{[1+4\alpha\beta(y-\lambda_2 h)]^{3/2}}{12\alpha^3\beta} \\ &+ \frac{h}{2a^2} + \frac{\beta h^2}{2a} - \frac{\beta(\lambda_2 h^2)}{a} - \frac{[1+4\alpha\beta(h-\lambda_2 h)]^{3/2}}{12a^3\beta} - v_p \Bigg] \end{aligned} \quad \text{(A.3.22)}$$

$$\begin{aligned} q_{outer} = w \Bigg[&-\frac{h^2-(\lambda_2 h)^2}{4\alpha^2} - \frac{\beta(h^3-(\lambda_2 h)^3)}{6\alpha} + \frac{\beta h^3 \lambda_2(1-\lambda_2^2)}{2\alpha} \\ &+ \frac{[1+4\alpha\beta(h-\lambda_2 h)]^{5/2}-1}{120\alpha^4\beta^2} + \frac{h^2(1-\lambda_2)}{2\alpha^2} + \frac{\beta h^3\lambda_2(1-\lambda_2)}{2\alpha} \\ &- \frac{(h-\lambda_2 h)[1+4\alpha\beta(h-\lambda_2 h)]^{3/2}}{12\alpha^3\beta} - v_p(h-\lambda_2 h) \Bigg] \end{aligned} \quad \text{(A.3.23)}$$

A.4 Solution for Plug Region (Region II)

As the shear rate does not change in the plug region as it can be seen from Figure A.4, velocity equations for inner and outer layer can be combined in this region.

Inner layer velocity ($y = \lambda_1 h$):

$$v_{plug,i} = \frac{\lambda_1 h}{2\alpha^2} - \frac{\beta(\lambda_1 h)^2}{2\alpha} + \frac{\beta(\lambda_1 h)^2}{\alpha} + \frac{\left[1 + 4\alpha\beta\left(\lambda_1 h - (\lambda_1 h)\right)\right]^{3/2}}{12\alpha^3\beta} - \frac{[1 + 4\alpha\beta(\lambda_1 h)]^{3/2}}{12\alpha^3\beta} \quad \text{(A.4.1)}$$

Rearrangement of equation above gives:

$$v_{plug,i} = \frac{\lambda_1 h}{2\alpha^2} + \frac{\beta(\lambda_1 h)^2}{2\alpha} + \frac{1}{12\alpha^3\beta} - \frac{[1 + 4\alpha\beta(\lambda_1 h)]^{3/2}}{12\alpha^3\beta} \quad \text{(A.4.2)}$$

Outer layer velocity ($y = \lambda_2 h$):

$$v_{plug,o} = -\frac{(\lambda_2 h)}{2\alpha^2} - \frac{\beta(\lambda_2 h)^2}{2\alpha} + \frac{\beta(\lambda_2 h)^2}{\alpha} + \frac{\left[1 + 4\alpha\beta\left((\lambda_2 h) - \lambda_2 h\right)\right]^{3/2}}{12\alpha^3\beta} + \frac{h}{2\alpha^2} + \frac{\beta h^2}{2\alpha} - \frac{\beta(\lambda_2 h^2)}{\alpha} - \frac{[1 + 4\alpha\beta(h - \lambda_2 h)]^{\frac{3}{2}}}{12\alpha^3\beta} - v_p \quad \text{(A.4.3)}$$

Rearrangement of equation above gives:

$$v_{plug,o} = -\frac{(\lambda_2 h)}{2\alpha^2} + \frac{\beta(\lambda_2 h)^2}{\alpha} + \frac{1}{12\alpha^3\beta} + \frac{h}{2\alpha^2} + \frac{\beta h^2}{2\alpha} - \frac{\beta(\lambda_2 h^2)}{\alpha} - \frac{[1 + 4\alpha\beta(h - \lambda_2 h)]^{\frac{3}{2}}}{12\alpha^3\beta} - v_p \quad \text{(A.4.4)}$$

As $v_{plug,i} = v_{plug,o}$, yields,

$$\frac{\lambda_1 h}{2\alpha^2} + \frac{\beta(\lambda_1 h)^2}{2\alpha} + \frac{1}{12\alpha^3\beta} - \frac{[1 + 4\alpha\beta(\lambda_1 h)]^{\frac{3}{2}}}{12\alpha^3\beta} = -\frac{(\lambda_2 h)}{2\alpha^2} + \frac{\beta(\lambda_2 h)^2}{\alpha} + \frac{1}{12\alpha^3\beta} + \frac{h}{2\alpha^2} + \frac{\beta h^2}{2\alpha} - \frac{\beta(\lambda_2 h^2)}{\alpha} - \frac{[1 + 4\alpha\beta(h - \lambda_2 h)]^{\frac{3}{2}}}{12\alpha^3\beta} - v_p \quad \text{(A.4.5)}$$

Gathering all terms of Equation A.4.5 in the right side gives,

$$-\frac{\lambda_1 h}{2\alpha^2} - \frac{\beta(\lambda_1 h)^2}{2\alpha} - \frac{1}{12\alpha^3\beta} + \frac{[1 + 4\alpha\beta(\lambda_1 h)]^{\frac{3}{2}}}{12\alpha^3\beta} - \frac{(\lambda_2 h)}{2\alpha^2} + \frac{\beta(\lambda_2 h)^2}{\alpha} + \frac{1}{12\alpha^3\beta} + \frac{h}{2\alpha^2} + \frac{\beta h^2}{2\alpha} - \frac{\beta(\lambda_2 h^2)}{\alpha} - \frac{[1 + 4\alpha\beta(h - \lambda_2 h)]^{\frac{3}{2}}}{12\alpha^3\beta} - v_p = 0 \quad \text{(A.4.6)}$$

Equation A.4.6 is the second equation which is going to be used in iterative procedure. The flow rate equation in this region can be written by using one of plug velocities determined above. To make calculations simpler, plug velocity belongs to inner layer is employed here with the following equations:

$$q_{plug} = v_{plug,i} wh(\lambda_2 - \lambda_1) \tag{A.4.7}$$

$$q_{plug} = wh\left(\frac{\lambda_1 h}{2\alpha^2} + \frac{\beta(\lambda_1 h)^2}{2\alpha} + \frac{1}{12\alpha^3\beta} - \frac{[1+4\alpha\beta(\lambda_1 h)]^{3/2}}{12\alpha^3\beta}\right)(\lambda_2 - \lambda_1) \tag{A.4.8}$$

A.5 Solution for Complete Slot

Total flow rate is the sum of determined flow rates for these three designated flow regions which is mathematically expressed with the following equation:

$$q_{total} = q_{inner} + q_{outer} + q_{plug} \tag{A.5.1}$$

Total flow rate will be used in mean velocity calculation. By replacing calculated Equations A.2.23, A.3.23, and A.4.8 into Equation A.5.1, total flow rate is found with the following equation.

$$\begin{aligned} q_{total} = w\Bigg\{&\left[\frac{(\lambda_1 h)^2}{4\alpha^2} - \frac{\beta(\lambda_1 h)^3}{6\alpha} + \frac{\beta(\lambda_1 h)^3}{2\alpha} + \frac{1-[1+4\alpha\beta(\lambda_1 h)]^{5/2}}{120\alpha^4\beta^2}\right. \\ &\left. - \frac{(\lambda_1 h)[1+4\alpha\beta(\lambda_1 h)]^{3/2}}{12\alpha^3\beta}\right] + \left[-\frac{h^2-(\lambda_2 h)^2}{4\alpha^2} - \frac{\beta(h^3-(\lambda_2 h)^3)}{6\alpha}\right. \\ &+ \frac{\beta h^3\lambda_2(1-\lambda_2^2)}{2\alpha} + \frac{[1+4\alpha\beta(h-\lambda_2 h)]^{5/2}-1}{120\alpha^4\beta^2} + \frac{h^2(1-\lambda_2)}{2\alpha^2} \\ &+ \frac{\beta h^3\lambda_2(1-\lambda_2)}{2\alpha} - \frac{(h-\lambda_2 h)[1+4\alpha\beta(h-\lambda_2 h)]^{3/2}}{12\alpha^3\beta} \\ &\left. - v_p(h-\lambda_2 h)\right] + h\left(\frac{\lambda_1 h}{2\alpha^2} + \frac{\beta(\lambda_1 h)^2}{2\alpha} + \frac{1}{12\alpha^3\beta}\right. \\ &\left. - \frac{[1+4\alpha\beta(\lambda_1 h)]^{3/2}}{12\alpha^3\beta}\right)(\lambda_2 - \lambda_1)\Bigg\} \end{aligned} \tag{A.5.2}$$

Mean velocity can be defined by following equation:

$$q_{total} = \bar{v} wh \tag{A.5.3}$$

Then,

$$\bar{v} = \left\{ \left[\frac{(\lambda_1 h)^2}{4\alpha^2} - \frac{\beta(\lambda_1 h)^3}{6\alpha} + \frac{\beta(\lambda_1 h)^3}{2\alpha} + \frac{1 - [1 + 4\alpha\beta(\lambda_1 h)]^{5/2}}{120\alpha^4\beta^2} \right.\right.$$
$$\left. - \frac{(\lambda_1 h)[1 + 4\alpha\beta(\lambda_1 h)]^{3/2}}{12\alpha^3\beta} \right] + \left[- \frac{h^2 - (\lambda_2 h)^2}{4\alpha^2} - \frac{\beta(h^3 - (\lambda_2 h)^3)}{6\alpha} \right.$$
$$+ \frac{\beta h^3 \lambda_2 (1 - \lambda_2^2)}{2\alpha} + \frac{[1 + 4\alpha\beta(h - \lambda_2 h)]^{5/2} - 1}{120\alpha^4\beta^2} + \frac{h^2(1 - \lambda_2)}{2\alpha^2} \qquad \text{(A.5.4)}$$
$$\left. + \frac{\beta h^3 \lambda_2 (1 - \lambda_2)}{2\alpha} - \frac{(h - \lambda_2 h)[1 + 4\alpha\beta(h - \lambda_2 h)]^{3/2}}{12\alpha^3\beta} - v_p(h - \lambda_2 h) \right]$$
$$\left. + h \left(\frac{\lambda_1 h}{2\alpha^2} + \frac{\beta(\lambda_1 h)^2}{2\alpha} + \frac{1}{12\alpha^3\beta} - \frac{[1 + 4\alpha\beta(\lambda_1 h)]^{3/2}}{12\alpha^3\beta} \right) (\lambda_2 - \lambda_1) \right\} / h$$

Equation A.5.4 is the last equation which is going to be used in the iterative procedure. As a result, Equations A.1.16, A.4.6 and A.5.4 will be solved concerning $\frac{dP_f}{dL}$, λ_1 and λ_2. As the developed equations are very complex in consideration of solving these equations for frictional pressure gradient is not possible, the python code based on the Trust Region Reflective algorithm is developed.

APPENDIX B

```
import math
import scipy.optimize as opt


h=0.042865  #change
k=0.46
ty=6.4201
vp=1.2192
vm=0.690622   #change
m=-0.0053
a=m/k


def f(p):
    # This is the function that we want to make 0

    # We take the unknowns

    (b,lamb1,lamb2) = p

    f1 = 2*ty/(h*(lamb2-lamb1))-b*k
    f2 = -vp+(1/(6*a*b)-h*lamb2+a*b*h**2*lamb2**2)/(2*a**2)-(-h-
a*b*h**2+2*a*b*h**2*lamb2+((1+4*a*b*(h-
h*lamb2))**(3/2)/(6*a*b)))/(2*a**2)+(1+4*a*b*h*lamb1)**(3/2)/(12*a**3*b)+(-1/(6*a*b)-
h*lamb1-a*b*h**2*lamb1**2)/(2*a**2)
    f3 = -vm+((lamb1**2*h**2)/(4*a**2)-
(a*b*lamb1**3*h**3)/(6*a**2)+(2*a*b*lamb1**3*h**3)/(4*a**2)+(1-
(1+4*a*b*lamb1*h)**(5/2))/(120*a**4*b**2)-
(lamb1*h*(1+4*a*b*lamb1*h)**(3/2))/(12*a**3*b)-(h**2-lamb2**2*h**2)/(4*a**2)-
(a*b*(h**3-lamb2**3*h**3))/(6*a**2)+(2*a*b*(lamb2*h**3-
lamb2**3*h**3))/(4*a**2)+((1+4*a*b*(h-lamb2*h))**(5/2)-1)/(120*a**4*b**2)-vp*(h-
lamb2*h)+(h**2-lamb2*h**2)/(2*a**2)+(a*b*(h**3-lamb2*h**3))/(2*a**2)-
(2*a*b*(lamb2*h**3-lamb2**2*h**3))/(2*a**2)-((h-lamb2*h)*(1+4*a*b*(h-
lamb2*h)**(3/2)))/(12*a**3*b))/h+((1-
(1+4*a*b*lamb1*h)**(3/2))/(12*a**3*b)+lamb1*h/(2*a**2)+a*b*lamb1**2*h**2/(2*a**2))*(l
amb2-lamb1)

    return [f1,f2,f3]


if __name__=="__main__":

    # We just call opt passing the function and an initial value
```

```
    solution = opt.least_squares(f,(1,0.3,0.5),bounds=((0,0,0),(math.inf,1,1)))
    print ("The solution is", solution)
```

CURRICULUM VITAE

Name Surname **: Mücahit YILDIZ**

Place and Date of Birth **: Konya, 04.08.1992**

E-Mail **: yildizmu@itu.edu.tr**

EDUCATION **:**

- **B.Sc.** **:** 2015, Istanbul Technical University, Faculty of Mines, Petroleum and Natural Gas Engineering

PROFESSIONAL EXPERIENCE AND REWARDS:

- 2017-2019, Research Assistant, Petroleum and Natural Gas Engineering Department, Istanbul Technical University